Fanconi anemia FANCD2 and FANCI proteins regulate the nuclear dynamics of splicing factors

María Moriel-Carretero,* Sara Ovejero,* Marie Gérus-Durand, Dimos Vryzas, and Angelos Constantinou

Institute of Human Genetics, Centre National de la Recherche Scientifique UMR 9002, Université de Montpellier, Montpellier, France

Proteins disabled in the cancer-prone disorder Fanconi anemia (FA) ensure the maintenance of chromosomal stability during DNA replication. FA proteins regulate replication dynamics, coordinate replication-coupled repair of interstrand DNA cross-links, and mitigate conflicts between replication and transcription. Here we show that FANCI and FANCD2 associate with splicing factor 3B1 (SF3B1), a key spliceosomal protein of the U2 small nuclear ribonucleoprotein (U2 snRNP). FANCI is in close proximity to SF3B1 in the nucleoplasm of interphase and mitotic cells. Furthermore, we find that DNA replication stress induces the release of SF3B1 from nuclear speckles in a manner that depends on FANCI and on the activity of the checkpoint kinase ATR. In chromatin, both FANCD2 and FANCI associate with SF3B1, prevent accumulation of postcatalytic intron lariats, and contribute to the timely eviction of splicing factors. We propose that FANCD2 and FANCI contribute to the organization of functional domains in chromatin, ensuring the coordination of DNA replication and cotranscriptional processes.

Introduction

Fanconi anemia (FA) is an autosomal and X-linked recessive disorder characterized by congenital abnormalities, severe bone marrow failure, and a high risk of developing acute myeloid leukemia and squamous cell carcinomas (Kee and D'Andrea, 2012; Kottemann and Smogorzewska, 2013). Bone marrow failure is caused by the attrition of the pool of hematopoietic stem/progenitor cells (Ceccaldi et al., 2012) that are highly sensitive to reactive aldehydes and to the overproduction of inflammatory cytokines (Haneline et al., 1998; Dufour et al., 2003; Garaycoechea et al., 2012).

The proteins mutated in FA exert a variety of functions in cellular stress responses that range from protection against replication-associated genomic instability and repair of DNA interstrand cross-links (ICLs) to antiviral responses and mitophagy (Räschle et al., 2008; Knipscheer et al., 2009; Schlacher et al., 2012; Laguette et al., 2014; Sumpter et al., 2016). To date, 21 FA proteins have been identified (Kottemann and Smogorzewska, 2013; Ceccaldi et al., 2016). During repair of ICLs, the DNA translocase FANCM anchors the multi-subunit ubiquitin ligase complex (FANCA, -B, -C, -E, -F, -G, and -L) to DNA damage sites (Deans and West, 2009; Yan et al., 2010). FANCD2 and FANCI are monoubiquitinated in the form of a DNA-bound heterodimer (Swuec et al., 2017; van Twest et al., 2017). FANCI is phosphorylated by ATM/ATR kinases on multiple residues to switch on FANCD2 monoubiquitination by the E2 ligase UBE2T (FANCT) and the E3 ligase FANCL (Meetei et al., 2004; Smogorzewska et al., 2007; Ishiai et al., 2008; Rickman et al., 2015). FANCD2 monoubiquitination is required for unhooking of the ICLs (Garcia-Higuera et al., 2001; Knipscheer et al., 2009). The repair of ICLs is achieved by the coordinated action of the structure-specific nuclease XPF (FANCQ) recruited by SLX4 (FANCP), the protein REV7 (FANCV) that participates in translesion DNA synthesis, and proteins implicated in homologous recombination, including BRCA1 (FANCS), BRCA2 (FANCD1), BRIP1 (FANCJ), PALB2 (FANCN), RAD51 (FANCR), RAD51C (FANCO), and XRCC2 (FANCU) (Kottemann and Smogorzewska, 2013; Ceccaldi et al., 2016).

In addition to ICL repair, the FA/BRCA pathway protects newly synthesized DNA from nucleolytic degradation (Schlacher et al., 2012; Lossaint et al., 2013) and mitigates interference between DNA replication and transcription-associated processes (Schwab et al., 2015; Madireddy et al., 2016). FANCI is a binding partner of FANCD2 (Smogorzewska et al., 2007). These 150- and 160-kD proteins are leucine rich and exhibit 150-aa sequence homology around their monoubiquitination sites (Smogorzewska et al., 2007). FANCD2 and FANCI adopt similar structures consisting essentially of α-helices arranged into α-solenoids (Joo et al., 2011). They have binding sites for both single-stranded and double-stranded DNA (Joo et al., 2011). It remains unclear how exactly FANCD2 and FANCI promote chromosomal stability when replication forks encoun-

*M. Moriel-Carretero and S. Ovejero contributed equally to this paper.

Correspondence to Angelos Constantinou: angelos.constantinou@igh.cnrs.fr

Abbreviations used: CSK, cytoskeleton; CV, column volume; DDR, DNA damage response; FA, Fanconi anemia; HU, hydroxyurea; IB, immunoblotting; ICL, interstrand cross-link; IF, immunofluorescence; IP, immune precipitate; PI, protease inhibitor; PLA, proximity ligation assay; SF, splicing factor; snRNP, small nuclear ribonuclear protein.

The Rockefeller University Press
J. Cell Biol. Vol. 216 No. 12 4007–4026
https://doi.org/10.1083/jcb.201702136

ter abnormal DNA structures or tightly chromatin-bound proteins. Upon activation of the master replication checkpoint kinase ATR, FANCD2 and FANCI accumulate in chromatin in the vicinity of replication forks, and FANCD2 associates transiently with the replicative helicase MCM2-7 (Lossaint et al., 2013; Panneerselvam et al., 2014; Chen et al., 2015). In addition, FANCD2 binds directly to histones and promotes nucleosome assembly (Sato et al., 2012), suggesting that FANCD2 regulates chromatin-based processes under stressful conditions.

To further explore the biological role of FANCI, we undertook proteomic and cell-biological approaches and identified FANCI-associated proteins in the nucleus. We found that FANCI associates with splicing factor 3B1 (SF3B1) throughout the cell cycle. FANCD2 also associates with SF3B1, but the proximity between the two proteins is restricted to chromatin in interphase. SF3B1 is a key subunit of the U2 small nuclear ribonucleoprotein (snRNP) required for the correct assembly of the splicing complex to the branch-point sequence (Gozani et al., 1998). This spliceosomal protein also tightly associates with chromatin, specifically with nucleosomes positioned over exons, and this independently of RNA (Kfir et al., 2015). SF3B1 is thought to transmit information conveyed by chromatin to the splicing machinery (Kfir et al., 2015).

Here we provide evidence that FANCD2 and FANCI promote the timely displacement of SF3B1 and the prototypical splicing factor (SF) SC35/SRSF2 from chromatin. Additionally, we find that FANCI specifically promotes the mobilization of SF3B1 and SC35 from nuclear speckles in response to ATR activation. Our findings reveal that FANCD2 and FANCI organize the nuclear dynamics of SFs.

Results

FANCI and FANCD2 stably associate with SF3B1

To gain further insights into the biological role of FANCI, we analyzed its protein–protein interaction network in chromatin. Flag-FANCI was stably expressed in human embryonic kidney (HEK293) cells. To induce its recruitment to chromatin, we exposed cells to hydroxyurea (HU), an inhibitor of ribonucleotide reductase that inhibits DNA synthesis through partial depletion of the dNTP pool. We prepared chromatin from HU-treated cells and then solubilized chromatin-bound proteins via extensive digestion of nucleic acids with benzonase, a pan-nuclease that degrades both RNA and DNA. Next, Flag-FANCI was captured on M2 agarose matrix and eluted with an excess of Flag peptide, and the resulting fractions were analyzed by mass spectrometry. STRING network analyses of FANCI-associated proteins revealed a strong enrichment in RNA-binding proteins and components of nuclear speckles/spliceosomes and nucleoli/ribosomes (Fig. S1 A).

We identified with a maximum number of peptides the spliceosomal protein SF3B1 and other subunits of the U2 snRNP. To confirm that FANCI associates with SF3B1, and to verify whether this could also happen in basal conditions, we performed coimmunoprecipitation experiments in the absence of HU. We prepared chromatin from HEK293 cells and digested it with benzonase to disrupt protein–protein interactions mediated by nucleic acids. We detected endogenous FANCI and FANCD2 in SF3B1 immune precipitates (IPs; Fig. 1 A) and reproduced the coimmunoprecipitation in the presence of ethidium bromide and RNase A (Fig. S1 B). These data indicate that the formation of protein complexes containing SF3B1, FANCI, or FANCD2 occurs in basal conditions and independently of nucleic acids. Consistent with this, Flag-FANCI and SF3B1 coeluted during fractionation of protein extracts by cation exchange chromatography through phosphocellulose followed by size-exclusion chromatography or affinity purification on M2 agarose (Fig. 1 B). Next, we coexpressed Flag-FANCD2, SF3B1-6His, and native FANCI in insect cells using recombinant baculoviruses. The three proteins coeluted during anti-Flag M2 agarose affinity chromatography (Fig. 1 C). Moreover, we performed immunoprecipitation with anti-SF3B1 (positive control), anti-FANCD2, and IgG (negative control) from HEK293 chromatin cell lysates and subjected them to RT-PCR. We detected the U2 snRNA in SF3B1 and FANCD2 IPs, whereas an unrelated tRNA was not detected (Fig. 1 D). Then, we used in situ proximity ligation assay (PLA) to verify that FANCD2 and FANCI are in proximity with SF3B1. We detected specific PLA signals between FANCI, FANCD2, and SF3B1 proteins in the nucleus of U2OS cells (Fig. 1 E). We performed a technical control in which each of the primary antibodies was substituted one at a time by an IgG antibody (Fig. 1 E). As biological controls, we used FA group D2 fibroblasts (PD20i) complemented or not with a cDNA encoding FANCD2 as well as U2OS cells treated with control or anti-FANCI siRNA (Fig. 1 F). Suppression of FANCD2 or FANCI proteins or omission of either one of the primary antibodies abolished PLA signals, validating the specificity of the results. Collectively, these data indicate that FANCD2 and FANCI associate with SF3B1 constitutively and localize in close proximity to SF3B1 in the nucleus.

The dynamics of SFs determines proximity between FANCI/FANCD2 and SF3B1

The proximity between FANCI/FANCD2 and SF3B1 led us initially to test whether SF3B1 is required for the formation of FANCD2 foci, FANCD2 monoubiquitination, and ICL repair. Control experiments revealed a significant decrease in cellular levels of FANCI and FANCD2 upon suppression of SF3B1 by RNAi. SF3B1 depletion also led to the decrease of FANCA (Fig. S1 C) and Chk1 levels (see Fig. 8 B). In contrast, other replication and repair proteins such as Nbs1, TopBP1, and PCNA were not significantly affected (Fig. S1 C). Treatment with the proteasome inhibitor MG132 did not rescue FANCI, FANCD2, and FANCA protein levels (Fig. S1 C). We did not detect FANCI and FANCD2 mRNAs in SF3B1-depleted cells (Fig. S1 D), indicating that the reduced protein level was the consequence of a defect in *FANCI* and *FANCD2* pre-mRNA processing. Consistent with this, expression of an intronless FANCI cDNA restored FANCI protein levels in SF3B1-depleted cells (Fig. S1 E). Collectively, these data indicate that SF3B1 is critical for expression of a subset of DNA damage response (DDR) proteins. SF3B1 thus contributes to the maintenance of chromosomal stability, at least indirectly.

Next, we used PLA in U2OS cells to define the context of the association between FANCD2, FANCI, and SF3B1. Intriguingly, the intensity of proximity signals between FANCI and SF3B1 was 10-fold stronger than between FANCD2 and SF3B1 (Figs. 1 E and 2 A). Extraction of nuclear soluble proteins using cytoskeleton (CSK) buffer did not affect PLA signals between FANCD2 and SF3B1, but reduced them between FANCI and SF3B1 to the level of FANCD2-SF3B1 proximity signals (Fig. 2 A). Thus, although both FANCD2 and FANCI associate

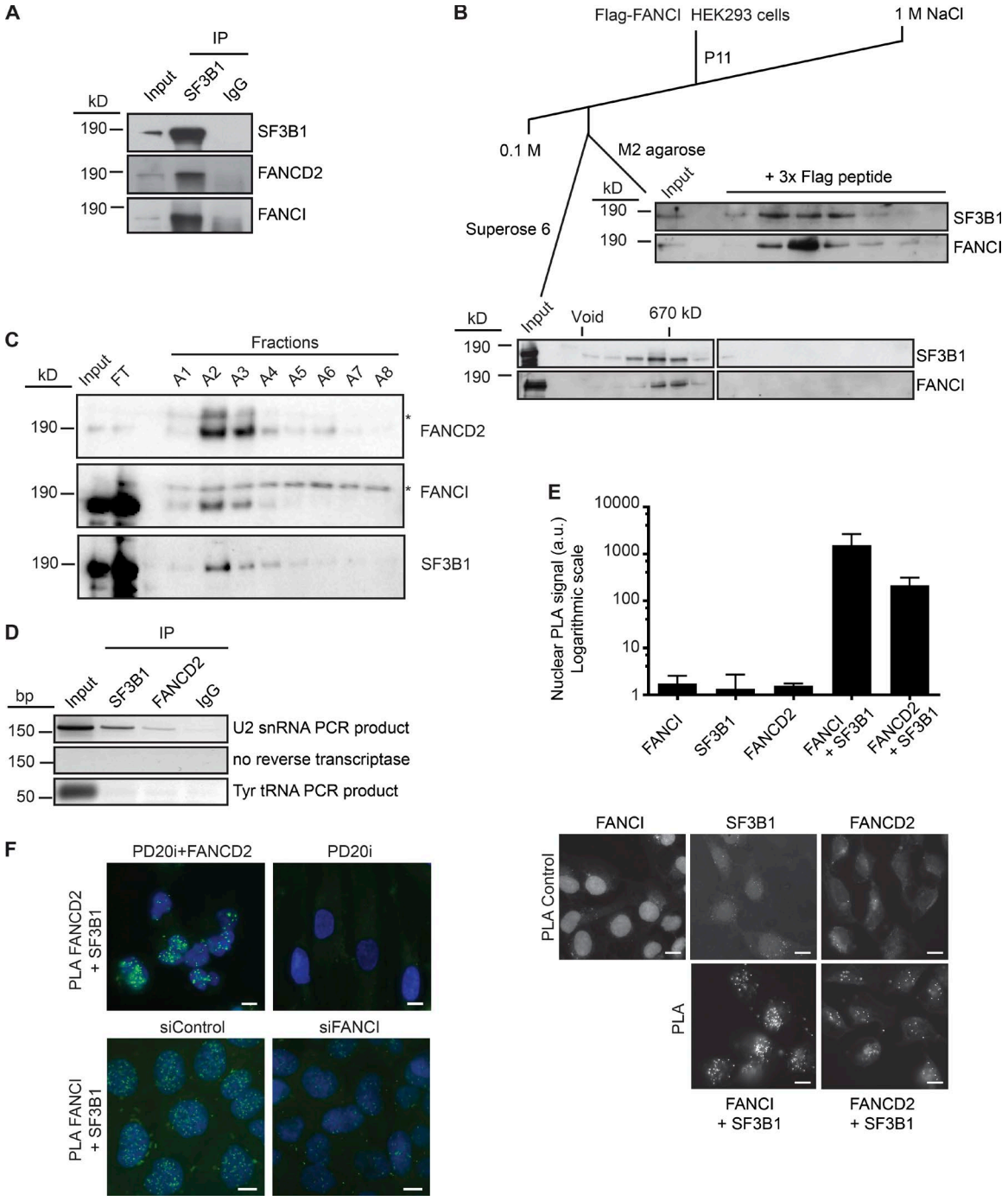

Figure 1. **FANCI and FANCD2 stably associate with SF3B1.** (A) FANCD2 and FANCI were probed by IB in SF3B1 IPs from HEK293 chromatin extracts. (B) Cell lysates from Flag-FANCI HEK293 cells were fractionated via P11, Superose 6, or M2 agarose chromatography and analyzed by IB. (C) Cells lysates from Sf21 insect cells expressing Flag-FANCD2, FANCI, and SF3B1-6His were fractionated by anti-Flag M2 agarose chromatography. FT, flowthrough. *, nonspecific bands. (D) SF3B1 and FANCD2 IP from HEK293 chromatin fraction were subjected or not to RT-PCR for U2 snRNA detection. Tyrosine (Tyr) tRNA was used as negative control. (E) PLAs in U2OS cells were performed using the indicated combinations of antibodies against FANCI, SF3B1, and FANCD2. The mean intensity of signals from three independent experiments (minimum of 200 cells each) is shown; error bars represent SD. DNA dyed with DAPI. (F) Biological control for PLA signals shown in E. (Top) PD20i cells complemented (PD20i + FANCD2) or not with FANCD2 cDNA (PD20i). (Bottom) siRNA-transfected U2OS cells. Bars, 10 µm.

with SF3B1 in chromatin, 90% of PLA signals between FAN CI and SF3B1 originate from the nucleoplasm. Because SF3B1 functions in splicing and most splicing occurs cotranscriptionally (Beyer and Osheim, 1988; Girard et al., 2012), we analyzed how transcription influences PLA signals between SF3B1, FANCD2, and FANCI. These signals were almost completely abolished after treatment with triptolide, an inhibitor of transcription initiation by RNA polymerase II (RNA PolII), or preextraction of soluble proteins with CSK buffer and RNA degradation by RNase A before fixation (Fig. 2 A). In agreement with these results, we detected RNA PolII in FANCI and FANCD2 IPs (Fig. S1 F). Thus, although FANCI, FANCD2,

and SF3B1 coimmunoprecipitate after extensive digestion of nucleic acids, PLA suggests that RNA and cotranscriptional splicing play important roles in the spatial organization of protein complexes containing FANCD2, FANCI, and SF3B1.

SFs are stored in speckles, which are self-assembled and nonmembranous dynamic organelles (Lamond and Spector, 2003). In interphase cells, the prototypical SF SC35 is distributed in chromatin and nuclear speckles. Upon entry into mitosis, SC35 is excluded from condensing chromatin until the anaphase–telophase transition and diffuses in the cytoplasm (Lamond and Spector, 2003; Fig. S2 A). PLA signals between FANCI and SF3B1 (Fig. 2 B, middle) mirrored the dynamics of SC35 during the cell cycle (Fig. 2 B, left). We detected mitotic FANCI-SF3B1 PLA signals in the cytoplasm (Fig. 2, middle; and Fig. S2 B). In contrast, FANCD2-SF3B1 PLA signals were not detected in mitotic cells but exclusively in the chromatin of interphase cells (Fig. 2 B, right; and Fig. S2 B). Hence, FANCD2 and FANCI exhibit distinct modes of association with SF3B1. The data so far indicate that FANCI associates with SF3B1 in chromatin and nucleoplasm during interphase and in the cytoplasm during mitosis, whereas the association between FANCD2 and SF3B1 is restricted to chromatin, most likely occurring during cotranscriptional splicing.

FANCI and FANCD2 regulate the mobility of prototypical SFs

The majority of transcription is suppressed during mitosis as a result of posttranslational modifications and chromosome hypercondensation (Johnson and Holland, 1965). To test whether FANCD2 and FANCI chromatin functions contribute to the timely eviction of SFs, we transfected U2OS cells with FANCI and FANCD2 siRNAs and visualized SC35 nuclear speckles in mitotic cells. Suppression of FANCI or FANCD2 did not perturb the level of SF3B1 and SC35 proteins (Fig. 2 C). In contrast, we noted that the level of FANCD2 was significantly reduced in FANCI knockdown cells (Fig. 2 C), as reported previously (Smogorzewska et al., 2007), whereas FANCI stability was not affected by the depletion of FANCD2 (Fig. 2 C). For each mitotic phase, we classified cells in three categories (from low to high) according to SC35 residual levels in chromatin and interchromatin granules, and we assigned each cell to one of them visually (Fig. 2 D). In control cells, we detected residual SC35 granules in the proximity of chromatin during prophase, whereas SC35 signals in chromatin diminished during prometaphase and metaphase (Fig. S2 A). In contrast, suppression of FANCI or FANCD2 increased the number of cells exhibiting medium or high levels of interchromatin granules and chromatin-associated SC35 in early mitosis compared with control cells (Fig. 2 E). These results indicate that the eviction of SC35 from condensing chromatin and its dispersion in the cytoplasm were delayed in FANCD2 and FANCI knockdown cells.

In search of complementary evidence that FANCD2 and FANCI influence the mobility of SF, we analyzed the structure and dynamics of nuclear speckles in interphase nuclei. A key function of nuclear speckles is to supply SFs to nearby active genes (Misteli et al., 1997). Because the depletion of FANCI or FANCD2 did not change the steady-state levels of SC35 and SF3B1 proteins (Fig. 2 C), we used the intensity of speckles marked by SC35 or SF3B1 immunofluorescence (IF) staining per whole nucleus as an indicator of the mobility of endogenous SF. To quantify defined SC35 speckles specifically, we extracted diffuse SC35 signals in the nucleoplasm via optical sectioning using ApoTome-structured illumination. Hence, the intensity of the remaining speckle signal is a direct reflection of the dynamics of SC35 and SF3B1 shuttling in and out of these bodies (Fig. 3 A, compare No Apo with Apo; see Materials and methods for more details). Automated analysis of hundreds of cells showed that suppression of FANCD2 reduced the intensity of SC35-marked speckles (Fig. 3, B and C; and Fig. S2, C and D), indicating that a greater proportion of SC35 remains outside of them in FANCD2-depleted cells. Suppression of FANCI had a similar impact on the localization of SC35, although to a milder extent (Fig. 3, B and C; and Fig. S2, C and D). Likewise, we analyzed the effect of FANCI and FANCD2 depletion on nuclear speckles marked by SF3B1 IF staining. In this case, suppression of FANCI slightly increased the retention of SF3B1 in nuclear speckles, whereas FANCD2 did not appear to have any consistent and significant impact on SF3B1 localization (Fig. 3, D and E; and Fig. S2, C and D). We obtained similar results using FANCD2 and FANCI siRNAs with different target sequences and from a distinct supplier (Fig. S2 E; depletion control in Fig. S3 A, lanes 1, 3, and 5).

In summary, our data indicate that FANCD2 and FANCI are required for the mobilization of SC35 from chromatin to speckles and FANCI for the release of SF3B1 from speckles in interphase. In addition, FANCD2 and FANCI are both required for the timely eviction of SFs from the nuclear environment in mitosis. Collectively, these data indicate that FANCI and FANCD2 influence the dynamics of SFs in the nucleus.

Accumulation of postcatalytic splicing intermediates and altered alternative splicing in FANCI/FANCD2-depleted cells

After completion of pre-mRNA splicing, intron-derived lariats and spliceosomes are disassembled to recycle snRNPs (Fourmann et al., 2013). The DHX15 helicase targets the U2 snRNP–intron interaction to promote the turnover of postcatalytic and stalled spliceosomes (Mayas et al., 2010; Fourmann et al., 2016). We originally detected DHX15 in FANCI-purified fractions by mass spectrometry and confirmed the presence of DHX15 in FANCD2 and FANCI IPs from chromatin fractions (Fig. S3 B). This prompted us to test whether FANCI or FANCD2 facilitate the removal of postcatalytic spliceosome and lariat degradation. To analyze this, we prepared total RNA from HEK293T cells and enriched intron lariats by virtue of their resistance to RNase R, a strong 3′-to-5′ exoribonuclease that leaves the circular part of intron-lariats intact (Suzuki et al., 2006). The efficiency of RNase R treatment was assessed by Northern hybridization of linear *GAPDH* mRNA (Fig. 4 A). Because SF3B1 associates with the branch-point adenosine in the pre-mRNA intron and promotes the assembly of a productive splicing complex (Corrionero et al., 2011), the proportion of RNase R-resistant molecules increased in SF3B1-depleted cells, as well as in the positive control cells lacking DHX15 (Fig. 4 A). Interestingly, we observed an accumulation of RNase R-resistant RNA species in cells treated with FANCD2 and FANCI siRNAs (Fig. 4 A). In contrast, the depletion of unrelated proteins, such as the phosphohydrolase SAMHD1 or the DNA integrity factor CTF18, had no impact on the accumulation of circular RNA (Fig. S3 C). We verified the efficiency of protein depletion by immunoblotting (IB; Fig. S3 D). These data indicate that suppression of FANCD2 or FANCI perturbs the timely disassembly of postcatalytic splicing intermediates in interphase cells, further confirming that these FA proteins influence the nuclear dynamics of SFs.

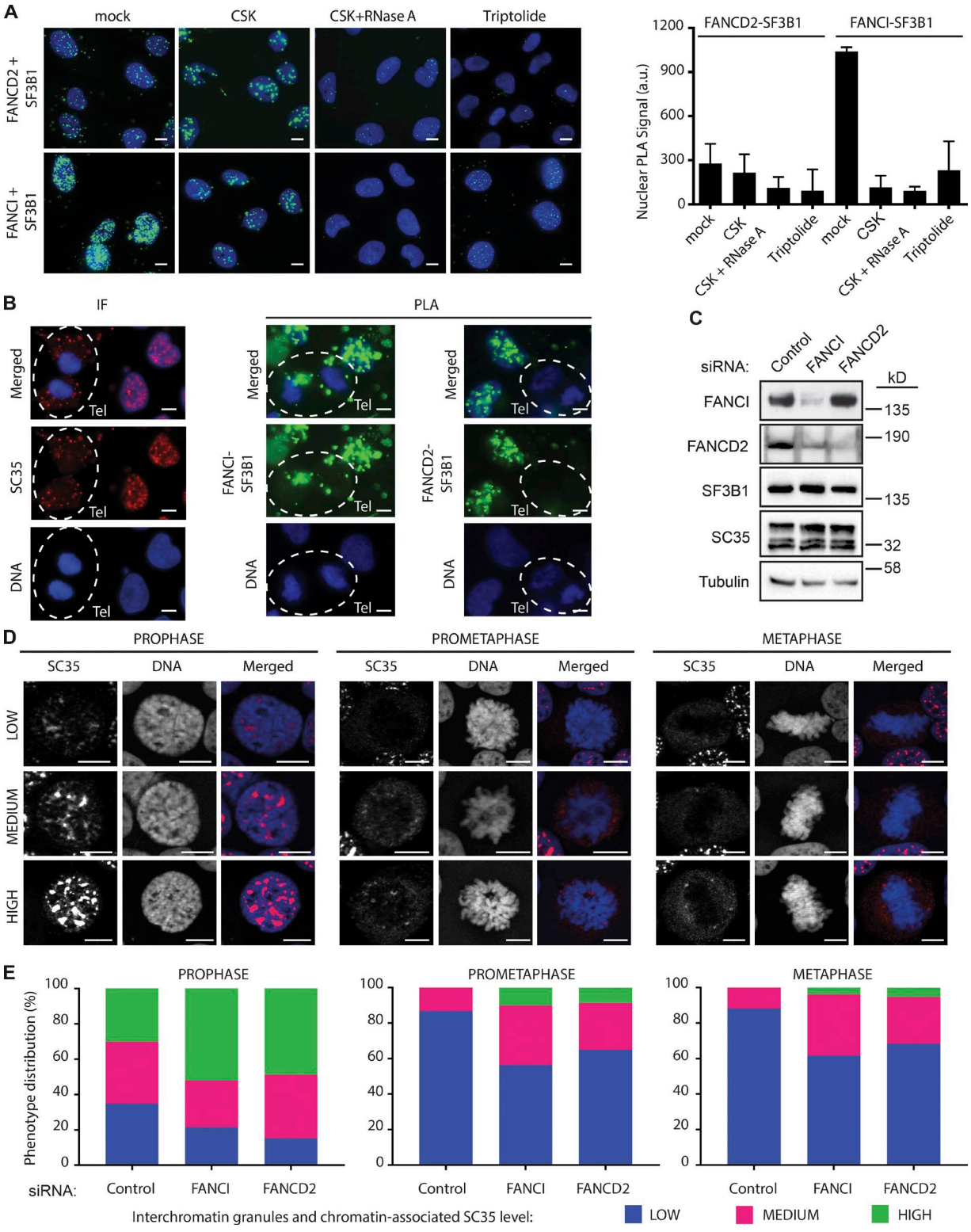

Figure 2. **The dynamics of SFs determines proximity between FANCI or FANCD2 and SF3B1.** (A) PLA signals (green) in U2OS cells preextracted or not with CSK buffer with or without RNase A, or after 1-h preincubation with 10 µM triptolide. (Right) Mean intensity of signals from three independent experiments (minimum of 200 cells each); error bars indicate SD. DNA (blue) dyed with DAPI. (B) SC35 (red) IF and PLA signals (green) in U2OS cells. DNA (blue) dyed with Hoechst. Discontinuous circles indicate telophases (Tel). (C) IB showing total levels of SF3B1 and SC35 proteins in siRNA-transfected U2OS cells. (D) Representative images of the three arbitrarily established categories indicative of the different intensities of SC35 levels in the initial three stages of mitosis. These categories were used to assign cells quantified in E. (E) SC35 speckles IF in siRNA transfected U2OS cells. Visual quantification from three independent experiments. For the final quantification, all mitoses counted for each category were added up (minimum of 50 cells/phase). Bars, 10 µm.

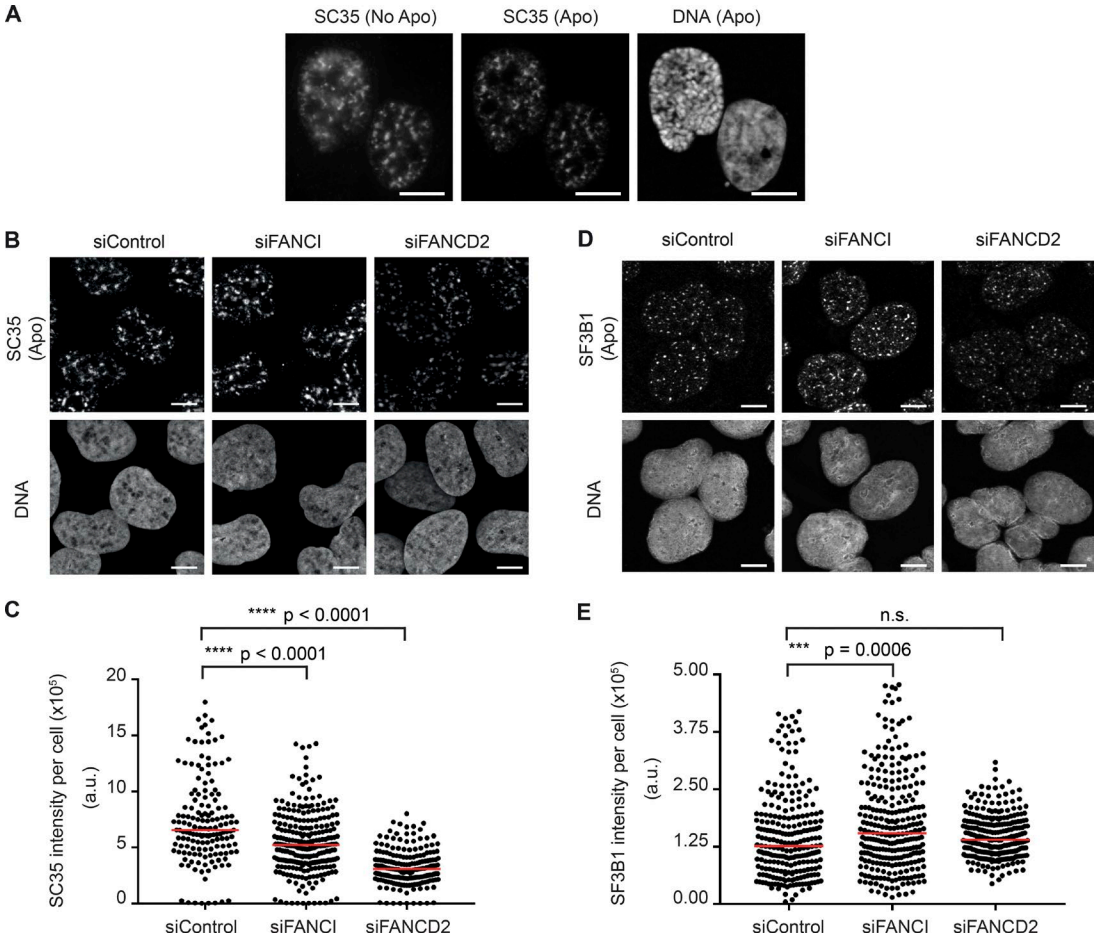

Figure 3. **FANCI and FANCD2 regulate the mobility of prototypical SFs.** (A) SC35 IF in U2OS cells. Image acquisition was performed in standard microscopy conditions (No Apo) or with ApoTome technology from Zeiss (Apo). (B and C) SC35 IF in siRNA-transfected U2OS cells. Image acquisition with ApoTome. Representative images are shown in B. Quantification of SC35 speckles intensity per cell. One representative experiment is shown in C; red bars mark the median value. *t* test significance is indicated by asterisks and *p*-value. The experiment was performed three more times (Fig. S2, C–E), with a minimum of 200 cells quantified per repetition. a.u., arbitrary units; n.s., not significant. (D and E) SF3B1 signal evaluated from the same experiment shown in B and C. Bars, 10 µm.

In summary, FANCD2 and FANCI differentially affect the subnuclear distribution of SF, yet suppression of both FANCI and FANCD2 induces the accumulation of lariats. To further understand how FANCD2 and FANCI influence pre-mRNA processing, we analyzed the consequences of FANCD2 and FANCI depletion on 12 representative splicing events that are determined by U2 snRNP concentration in the vicinity of the spliced mRNA (Xiao et al., 2012). Conditioned by the relative strength of splicing sites within the introns, low local U2 snRNP concentration always leads to decreased exon inclusion, whereas increased local U2 snRNP concentration can yield both exon inclusion or exclusion (Xiao et al., 2012). Consistent with this, suppression of SF3B1 decreased exon inclusion in the 12 mRNAs that were initially identified as responsive to the depletion of SF3A2, another subunit of U2 snRNP (Xiao et al., 2012; Fig. 4, B and C). In FANCI-depleted cells, we observed a reduction of exon inclusion in half of these mRNAs, consistent with a decrease in the local concentration of U2 snRNP (Fig. 4 C, red bars). In FANCD2-depleted cells, we also observed alterations in some mRNAs that included both a diminution (*HHLA3*, *ATXN2*, *ECHDC1*, and *DAB2)* or an increase (*FAM62B*, *PSMG1*, and *ABI2*) in exon inclusion, suggestive of an increase in the local concentration of U2 snRNP (Fig. 4 C, orange bars). We repeated this analysis in HEK293T cells and observed similar trends, although the effects were less pronounced (Fig. S3 E). These data suggest that regulation of the dynamics of SFs by FANCI and FANCD2 has an impact on splicing outcomes.

FANCI and FANCD2 exhibit distinct association patterns with indicators of splicing events

To further explore how FANCD2 and FANCI differentially regulate splicing outcomes, we analyzed the association of FANCI and FANCD2 with components of the spliceosome that act in early and late steps of pre-mRNA splicing. We found that FANCI and FANCD2 associate with the postcatalytic spliceosome dismantler DHX15 (Fig. S3 B). DHX15, however, is also present in early spliceosomes (Agafonov et al., 2011). Thus, we studied the interaction of FANCI and FANCD2 with three other spliceosome components: SPF45, whose distribution in spliceosomal complexes mirrors exactly that of DHX15 at very early stages (Agafonov et al., 2011); TFIP11, exclusively present during disassembly of postcatalytic spliceosomes (Tanaka et al., 2007; Wen et al., 2008; Yoshimoto et al., 2009); and PRP8, a key and central splicing component (Agafonov et al., 2011).

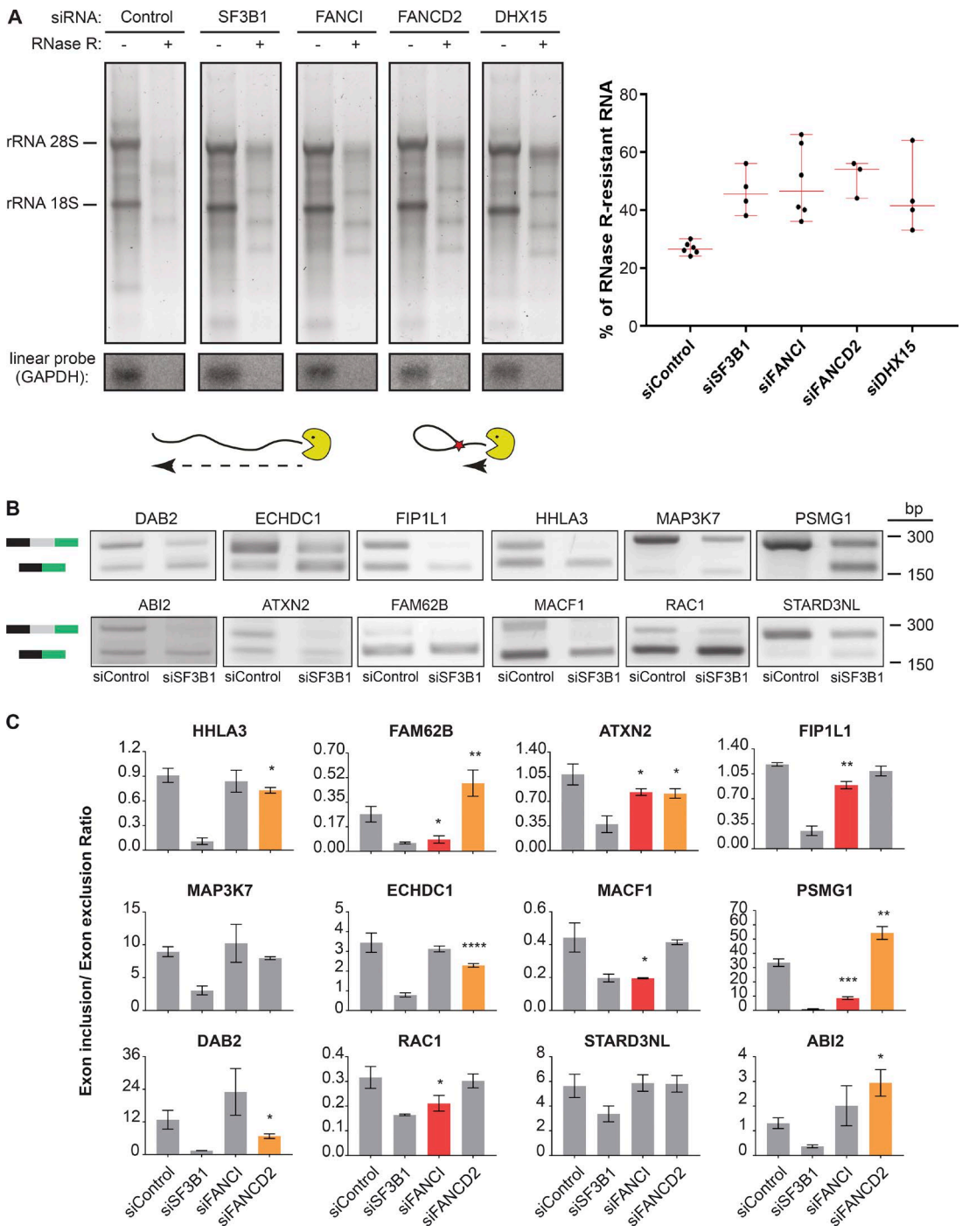

Figure 4. **FANCI or FANCD2-depleted cells accumulate postcatalytic splicing intermediates.** (A) Total RNA from siRNA-transfected HEK293T cells was digested or not with RNase R. Northern blot of linear *GAPDH* mRNA was used as control of RNase R digestion efficiency. Quantification of at least three different experiments shows the ratio of RNAs resistant to digestion (indicative of circular RNA, lane +) versus total RNA (lane –) as percentages. Red bars indicate the maximum, median, and minimum values. (B) Validation of SF3B1 depletion effect on alternative splicing. RT-PCR on total RNA from siRNA-transfected U2OS cells shows mature mRNAs containing either three exons (top band) or the two flanking ones (bottom band). (C) Ratio between exon inclusion and exon exclusion from at least three independent experiments from SF3B1-, FANCI-, or FANCD2-depleted U2OS cells. Error bars indicate SD. *t* test statistically relevant values are highlighted in red for siFANCI and in orange for siFANCD2 (****, $P < 0.0001$; ***, $P < 0.001$; **, $P < 0.01$; *, $P < 0.1$).

We detected DHX15 and the early spliceosomal protein SPF45 in Flag-FANCI IPs, whereas the mid- and late-acting factors PRP8 and TFIP11 were not enriched in Flag-FANCI pull-downs (Fig. 5 A, compare lanes 3 and 4). PLA yielded concordant results (Fig. 5 B). In contrast, FANCD2 coimmunoprecipitated with DHX15 and the late acting factor TFIP11, but not with the early and mid-acting factors SPF45 and PRP8 (Fig. 5 C, compare lanes 3–4 and 5–6). Induction of FANCD2 recruitment to chromatin by treatment with HU did not alter this pattern (Fig. 5 C). We did not observe PLA signals between FANCD2 and any of these SFs, perhaps as a consequence of the spatial organization of the proteins (Fig. 5 B).

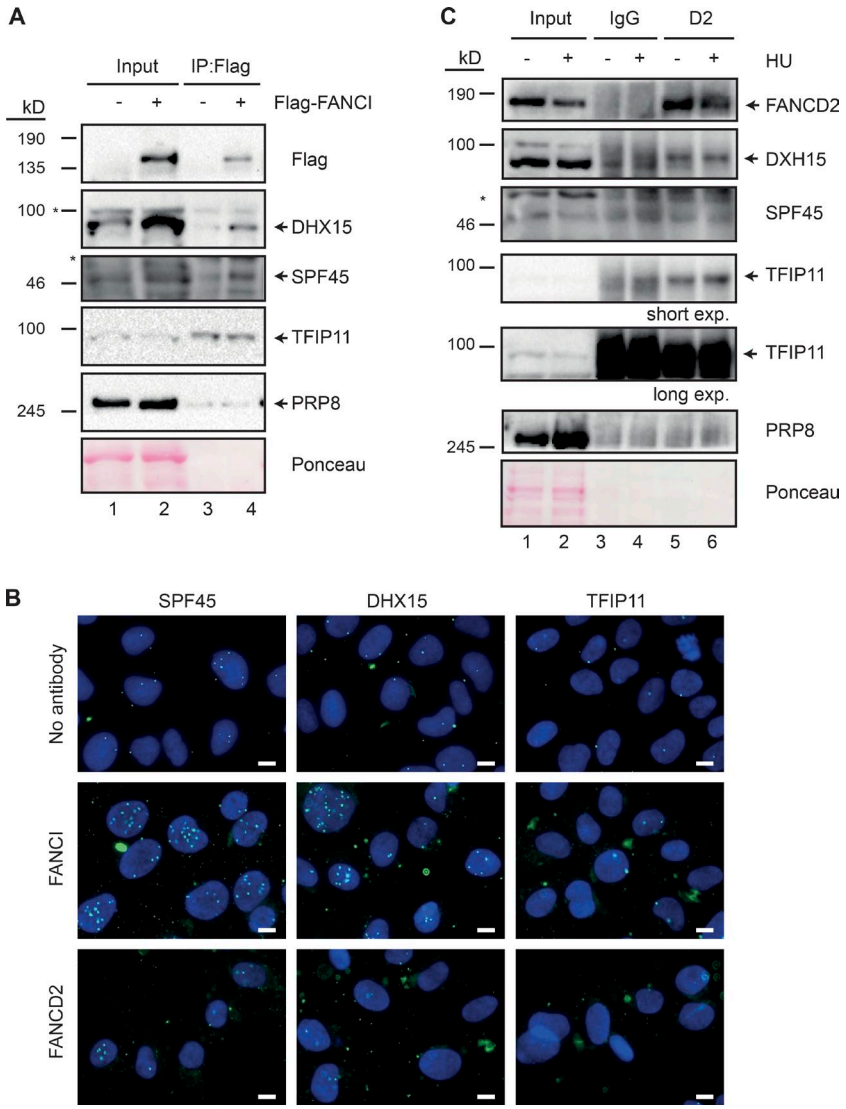

Figure 5. **Different contribution of FANCI and FANCD2 to splicing catalysis timing.** (A) Flag IP from chromatin extract of HEK293 WT (–) or Flag-FANCI stable cells (+). IB of DHX15, SPF45, TFIP11, and PRP8. *, unspecific band. (B) PLA signals (green) in U2OS cells using indicated combinations of antibodies. DNA (blue) dyed with DAPI. (C) FANCD2 IP from chromatin extract as in A. Cells were treated or not with 5 mM HU for 1 h. IB of DHX15, SPF45, TFIP11, and PRP8. IgG IP, negative control. *, unspecific band. Bars, 10 µm.

These observations suggest that FANCI facilitates the engagement of SFs in pre-mRNA splicing, consistent with a diminution of the local concentrations of U2 snRNP in FANCI-depleted cells. In contrast, FANCD2 may contribute to the disassembly and eviction of postcatalytic spliceosomes, in agreement with an increase in the local concentrations of U2 snRNPs in FANCD2-depleted cells.

Replication stress promotes the release of SFs from speckles in an ATR-dependent manner

The release of SFs from speckles is regulated by Ser/Thr protein kinases (Misteli et al., 1997; Sacco-Bubulya and Spector, 2002). Furthermore, FANCI phosphorylation on Ser/Thr-Gln motifs by the replication checkpoint kinase ATR is required for the activation of the FA pathway and for the stabilization of FANCD2 and FANCI on chromatin (Ishiai et al., 2008). Thus, we tested whether the Ser/Thr kinase ATR influences the nuclear organization of SFs. We induced ATR activation in U2OS cells by treatment with the replication inhibitor HU, as indicated by the phosphorylation of its downstream target kinase Chk1 on Ser345 (Fig. S4 A). Quantification of the intensity of SC35-marked speckles after optical sectioning revealed that the exposure of U2OS cells to HU for 5 min induces a significant decrease in the intensity of speckles labeled by SC35 staining (Fig. 6 A, top; and Fig. S4 A). This phenomenon persisted after 1-h treatment with HU (Fig. 6 A, top; and Fig. S4 A). Likewise, the intensity of speckles labeled with SC35 also diminished in nontumoral RPE1-hTERT cells and HeLa S3 cells exposed to HU for 60 min (Fig. 6 A, middle and bottom; and Fig. S4, B and C). The intensity of SF3B1-marked speckles was also reproducibly reduced in U2OS cells treated with HU for 5 min (Fig. S4 D). This effect was concomitant with an increase in chromatin-bound SF3B1 visualized by IF after extraction of soluble proteins using CSK buffer (Fig. 6 B). Chromatin-bound SF3B1 also increased in cells exposed to aphidicolin, an inhibitor of DNA polymerase α (Fig. 6 B), indicating that inhibitors of DNA replication induce the retention of SFs in chromatin. Consistent with the release of SF3B1 from speckles being an early response to HU treatment, changes in the intensity of speckles labeled with SF3B1 were less pronounced after U2OS, RPE1-hTERT, or HeLa S3 cell lines were exposed to HU for 1 h (Fig. 6 C and Fig. S4, D–F). Using a specific inhibitor of ATR (Fig. 6 D; treatment control in Fig. S5 A), VE-821, we observed that the activity of ATR was required to induce the release of SFs from speckles in response to the exposure of

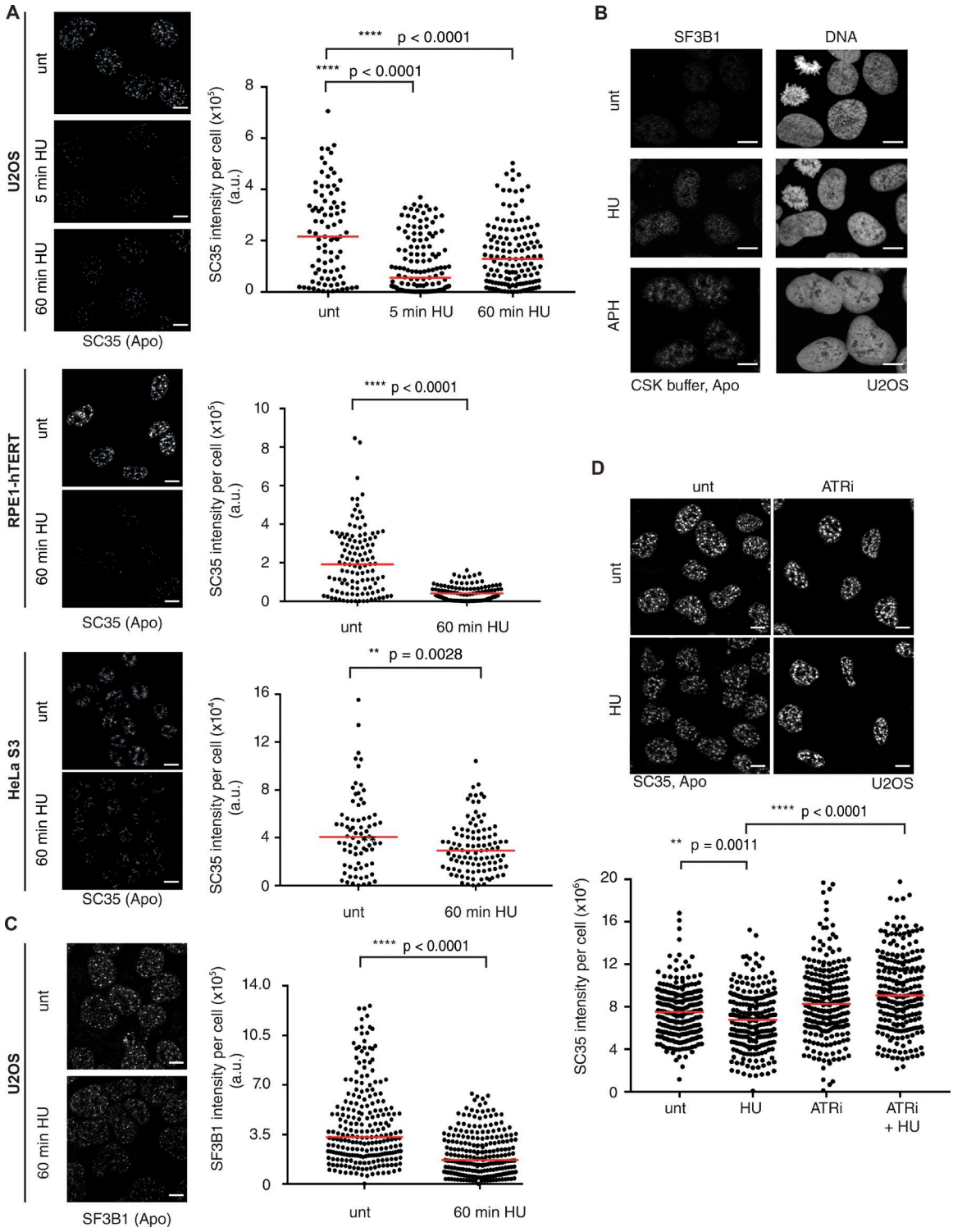

Figure 6. **SFs dynamics is controlled by ATR in response to HU-induced replication stress.** (A) SC35 IF in U2OS (top), RPE1-hTERT (middle), or HeLa S3 (bottom) cells treated with 5 mM HU for 5 or 60 min. Quantification performed as described in Fig. 3; minimum 100 cells. (B) SF3B1 IF in CSK preextracted U2OS cells treated with 5 mM HU for 60 min or 0.3 µM aphidicolin (APH) for 16 h. (C) The same experiment as in A to detect SF3B1. (D) SC35 IF in U2OS cells pretreated or not with 10 µM VE-821 (ATRi) for 2 h followed by 5 mM HU for 60 min. Quantifications and statistics as in Fig. 3. One representative experiment and its corresponding images are shown; Fig. S5 B shows the median of this experiment and three additional biological replicates. Bars, 10 µm.

U2OS cells to HU (Figs. 6 D and S5 B). In conclusion, these results indicate that ATR activation promotes the mobilization of SFs from nuclear speckles to chromatin in response to replication inhibition by HU.

FANCI and FANCD2 promote the relocalization of SFs upon DNA replication stress

To analyze whether and how inhibition of DNA replication influences the association between FANCD2, FANCI, and SF3B1,

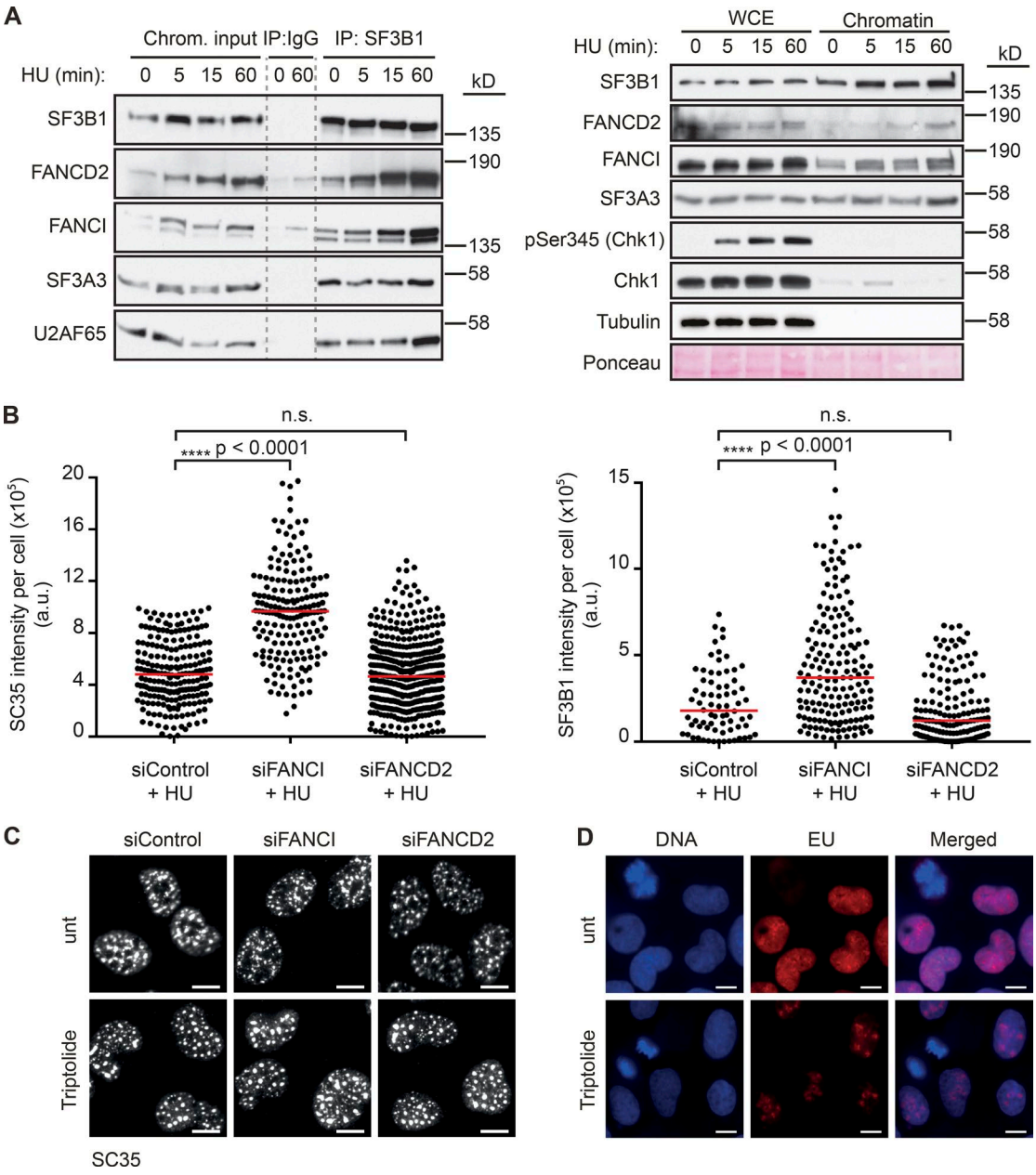

Figure 7. **FANCI and FANCD2 promote the relocation of SFs upon DNA replication stress.** (A) SF3B1 IP from chromatin extracts prepared from HEK293 cells treated with 5 mM HU for the indicated times. IB of FANCI, FANCD2, SF3A3, and U2AF65. (Left) Inputs and IPs; right, whole-cell extracts (WCE) versus chromatin inputs. (B) Representative experiment of SC35 and SF3B1 quantifications in siRNA-transfected U2OS cells treated with 5 mM HU for 1 h. Quantifications as in Fig. 3 from at least three repetitions on a minimum of 120 cells. (C) SC35 IF in siRNA-transfected U2OS cells treated with 10 µM triptolide for 1 h. (D) 10-min EU incorporation in triptolide-treated siControl cells used in C. Bars, 10 µm.

we prepared chromatin at different time points during HU treatment, solubilized chromatin-bound proteins with the pan-nuclease benzonase, and immunoprecipitated endogenous SF3B1 (Fig. 7 A, left). We probed Chk1 phosphorylation on Ser345 by IB to verify the efficacy of ATR activation by HU (Fig. 7 A, right). As expected, FANCI and FANCD2 accumulated on chromatin during the course of exposure to HU (Fig. 7 A). The amount of FANCD2 and FANCI detected in SF3B1 IPs increased with incubation time in HU, whereas levels of the SFs SF3A3 and U2AF65 pulled down with SF3B1 remained almost constant throughout the time-course analysis (Fig. 7 A, left). This result indicates that during the course of treatment with HU, FANCD2 and FANCI accumulate on chromatin in proximity to SF3B1.

To test whether FANCD2 or FANCI also influences the dynamics of SFs in response to HU, we quantified the intensity of SC35 and SF3B1 signals in speckles using images acquired by optical sectioning. The efficacy of FANCD2 and FANCI depletion and the induction of Chk1 phosphorylation by HU are shown in Fig. S5 C. Suppression of FANCD2 in HU-treated cells did not alter the size and intensity of nuclear speckles (Fig. 7 B). The amount of SFs stored in speckles diminished when cells were treated with either an anti-FANCD2 siRNA or HU (Figs. 3 and 6, respectively). This result indicates that the combination of HU and FANCD2 depletion has no additive effect on the localization of SF. In contrast, suppression of FANCI in HU-treated cells yielded significantly larger speckles

in comparison with control cells (Fig. 7 B). We confirmed these observations using siRNAs with distinct targeting sequences (Fig. S5, D and E, green dots; depletion and treatment control in Fig. S3 A). The overall analysis of speckles marked by SC35 or SF3B1 staining indicates that FANCI, but not FANCD2, promotes the mobilization of SFs from nuclear speckles in response to HU. This is consistent with the observation that FANCI and SF3B1 yield strong PLA signals in the nucleoplasm, whereas proximity between FANCD2 and SF3B1 is restricted to chromatin (Fig. 2 A). Upon inhibition of transcription, SFs accumulate in nuclear speckles, which consequently become larger and more rounded (Misteli et al., 1997). Consistent with proximity between FANCD2, FANCI, and SF3B1 depending on transcription activity or its product RNA (Fig. 2 A), the depletion of neither FANCI nor FANCD2 altered the rounding and size increase of speckles induced by the transcription inhibitor triptolide (Fig. 7 C; treatment control in Fig. 7 D). Collectively, these data indicate that FANCI and FANCD2 influence the dynamics of SFs in coordination with transcription.

FANCD2 and FANCI regulate the dynamics of SFs independently of the FA core complex

FANCD2 monoubiquitination by the FA core complex is essential for activation of the FA/BRCA pathway in response to DNA damage and for replication-coupled repair of ICLs (Garcia-Higuera et al., 2001; Knipscheer et al., 2009). Thus, we destabilized the FA core complex via the knockdown of its key subunit FANCA to test whether FANCD2 monoubiquitination is necessary for FANCD2 function in the regulation of SF dynamics. The size of speckles labeled with SC35 or SF3B1 increased in FANCA knockdown cells (Fig. 8, A and B), a pattern that is opposite to that observed in FANCD2 knockdown cells (Fig. 3, B–E). Furthermore, suppression of FANCA slightly perturbed the ratio of exon inclusion/exclusion of only two genes, *HHLA3* and *FAM62B* (Fig. 8 C, red bars), in a way that was opposite to that observed in FANCD2-depleted cells (Figs. 4 C and S3 E). Likewise, suppression of FANCA had minor impact on the ratio of exon inclusion/exclusion in HU-treated cells (Fig. 8 C, orange bars). Suppression of FANCA had no impact on HU-induced release of SC35 and SF3B1 from nuclear speckles (Fig. 8 A), an event that is dependent on FANCI (Fig. 7 B). Collectively, these observations suggest that FANCD2 and FANCI regulate the dynamics of SFs independently of the FA core complex. Suppression of FANCA, however, is likely to modify the equilibrium of the pools of FANCD2 associated with SFs and FANCD2 engaged in DNA repair, consistent with the observation that FANCA depletion and FANCD2 depletion have opposite effects on the dynamics of SFs.

ATR-mediated phosphorylation of FANCI contributes to the mobility of SFs

Because we observed that the release of SFs from speckles is ATR and FANCI dependent (Figs. 6 D and 7 B), we analyzed whether FANCI was the predominant effector of ATR in this process. To test this, we overexpressed in U2OS cells a nonphosphorylatable mutant version of FANCI, EGFP-Flag-FANCI^{6SA}, that carries serine-to-alanine substitutions at the six S/T-Q ATR-consensus sites (Chen et al., 2015; Fig. 9 A). We maintained these cells in culture for 1 mo and analyzed nuclear speckles every week (Fig. 9 B, E1–E3). In basal condition, the size of nuclear speckles labeled with SC35 or SF3B1 gradually diminished in cells expressing either EGFP-Flag FANCI^{WT} or EGFP-Flag-FANCI^{6SA} (Fig. 9, B and C), consistent with the conclusion drawn from siRNA experiments that FANCI promotes the release of SFs from speckles (Fig. 3, C and E; and Fig. 7 B). Next, we used RNA interference to produce cell lines that express either FANCI^{6SA} or FANCI^{wt} (Fig. 9 A). HU treatment induced the release of SC35 and SF3B1 from nuclear speckles in cells expressing FANCI^{wt}, as expected, whereas the impact of HU on the mobility of SFs was less pronounced in cells expressing FANCI^{6SA} (Fig. 9 D). We conclude that FANCI phosphorylation by ATR in response to treatment with HU contributes to the release of SFs from nuclear speckles.

Discussion

FANCD2 and FANCI accumulate in DNA damage–induced chromatin foci and have a well-characterized function in the repair of ICLs. In contrast, the cellular physiology of non–DNA-bound FANCD2 and FANCI remains poorly defined. Here we present evidence that FANCD2 and FANCI are organized in the nucleus in close proximity to the spliceosomal U2 snRNP. Our data indicate that FANCD2 and FANCI regulate the dynamic redistribution of SFs between nuclear speckles and chromatin. This study defines a previously uncharacterized role for FANCD2 and FANCI in cotranscriptional processes, with important implications for cellular homeostasis and chromosome stability.

The FA proteins have not been identified in proteomic analyses of nuclear speckles or the pre-mRNA splicing machinery. Yet FANCD2 and FANCI copurified with SF3B1 and yielded PLA signals with SF3B1 in the nucleus. A previous study showed that FANCI interacts with a ubiquitin-like protein implicated in pre-mRNA splicing, UBL5, which is thought to promote the function of FANCI in ICL repair independently of its splicing function (Oka et al., 2015). Here we were unable to decipher whether SF3B1 exerts a function in ICL repair because suppression of SF3B1 led to the depletion of FANCI and FANCD2 (Fig. S1, C–E). Indeed, components of the U2 snRNP are essential to ensure the stability of several DNA repair proteins (Tanikawa et al., 2016). Likewise, the SF RBMX is required for BRCA2 and ATR stability (Adamson et al., 2012). Splicing inhibitors impair the DDR via down-regulation of the E3 ubiquitin ligase RNF8 (Pederiva et al., 2016). Thus, the DDR is highly sensitive to the deregulation of SFs. Yet, the association of DDR proteins and SFs may influence transcription and pre-mRNA splicing. For example, BRCA1 forms a complex with SFs upon DNA damage and promotes the expression of proteins involved in the DDR (Savage et al., 2014). We show here that FANCD2 and FANCI regulate the spatial organization of SFs in both interphase and mitotic cells, although the precise mechanism by which they do so has yet to be explored.

Intriguingly, the most abundant proteins isolated with FANCI were components of nucleoli and nuclear speckles (Fig. S1 A). These membraneless organelles form via liquid–liquid phase transitions driven by proteins such as NPM1, which can phase-separate into liquid droplets under physiological protein and salt concentrations (Feric et al., 2016; Marzahn et al., 2016). The nuclear speckle marker SC35 binds to liquid droplets formed by hnRNPA1, and this is reversed by CLK1/2-mediated phosphorylation of its S/R-rich domain (Kwon et al., 2014). The association of FANCI and FANCD2 with nucleolar and splicing proteins and their contribution to the spatial

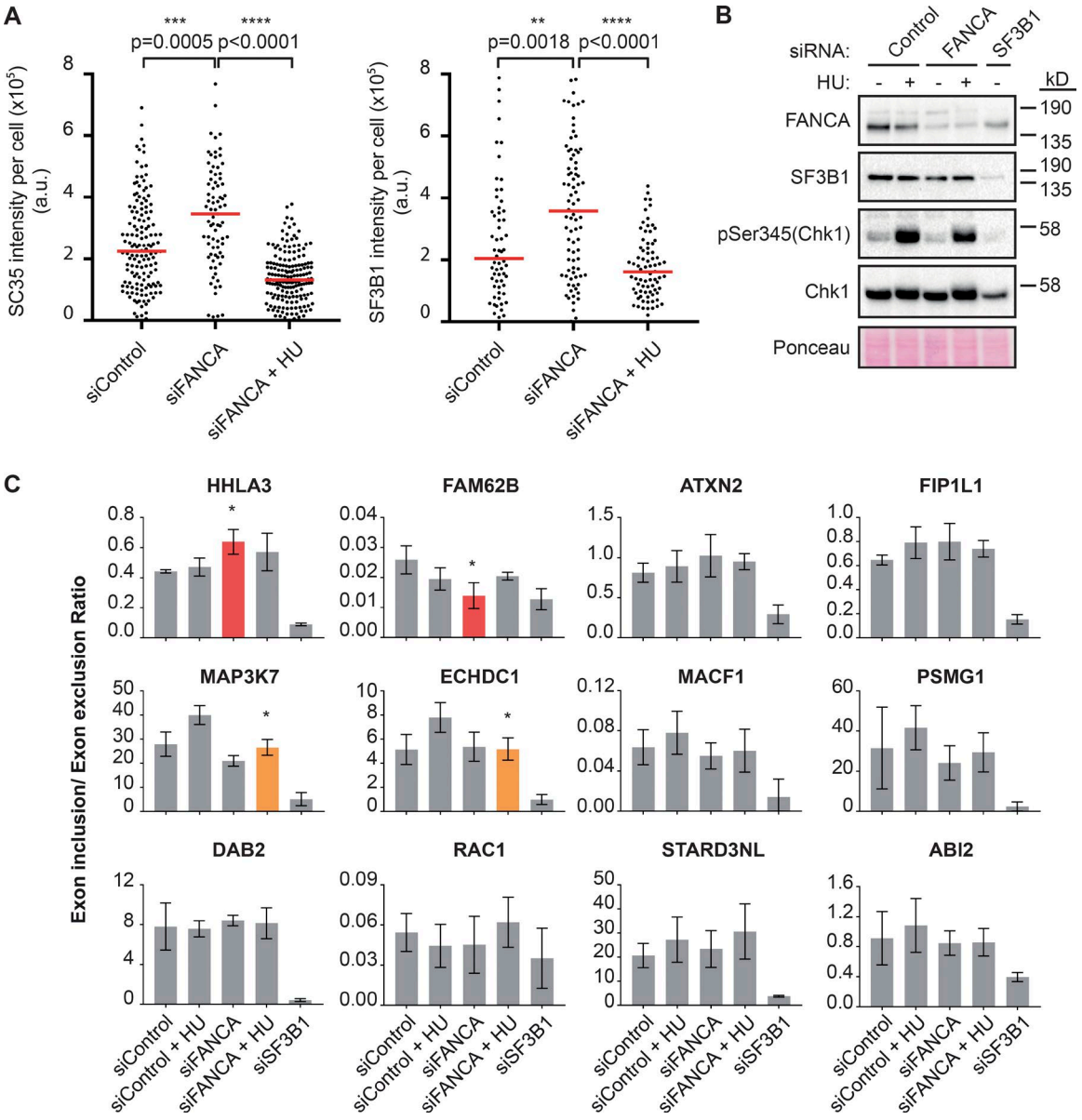

Figure 8. **FANCA does not play a major role in the dynamics of SFs.** (A) SC35 and SF3B1 IF representative experiment (n = 3) in siRNA-transfected U2OS cells treated or not with 5 mM HU for 1 h. Quantifications as in Fig. 3 on a minimum of 120 cells. (B) IB control for A and C showing FANCA and SF3B1 depletion upon siRNA transfection and efficiency of HU treatment (pSer345Chk1). (C) Quantifications of FANCA depletion and HU treatment impact on alternative splicing in U2OS cells from three biological replicates (n = 3), ≥120 cells each. Cells were treated as described in A. Quantifications as in Fig. 4 C. *t* test statistically relevant values, compared with siControl, are highlighted in red for siFANCA and orange for siFANCA + HU (*, 0.01 < P < 0.1).

distribution of SC35 and SF3B1 suggest that these FA proteins interface with membraneless structures and influence the dynamic exchange of their constituent molecules.

We observed notable differences between FANCD2 and FANCI, consistent with evidence suggesting that FANCD2 and FANCI can function independently of each other (Sareen et al., 2012; Castella et al., 2015). First, FANCI and SF3B1 yielded strong PLA signals throughout the cell cycle, in both the nucleoplasm of interphase cells and the cytoplasm of mitotic cells, whereas PLA signals between FANCD2 and SF3B1 were restricted to the chromatin of interphase cells (Fig. 2, A and B; and Fig. S2 B). In line with this observation, the pool of SF3B1, which is reported to be mainly chromatin bound (Girard et al., 2012), becomes associated with speckles in the absence of FANCI. Given that SF3B1 associates with nucleosomes until its engagement in intron processing (Kfir et al., 2015) and that FANCD2 possesses a histone chaperone function (Sato et al., 2012), one possibility is that FANCD2 regulates the activity or the association of chromatin-bound SC35 and SF3B1 with other proteins. Second, ATR activation by cellular treatment with HU induces the release of SC35 and SF3B1 out of speckles, whereas both proteins accumulate in them only in FANCI-depleted cells exposed to HU. We provide evidence that FANCI phosphorylation contributes to the release of SFs in response to ATR activation, suggesting that FANCI functions as an effector of ATR in this process. Third, we observed that FANCI associates with proteins that act early in pre-mRNA splicing, whereas FANCD2 immunoprecipitates with post-catalytic SF. The phenotypic consequences of FANCI depletion are consistent with low levels of U2 snRNP in the vicinity of splicing substrates,

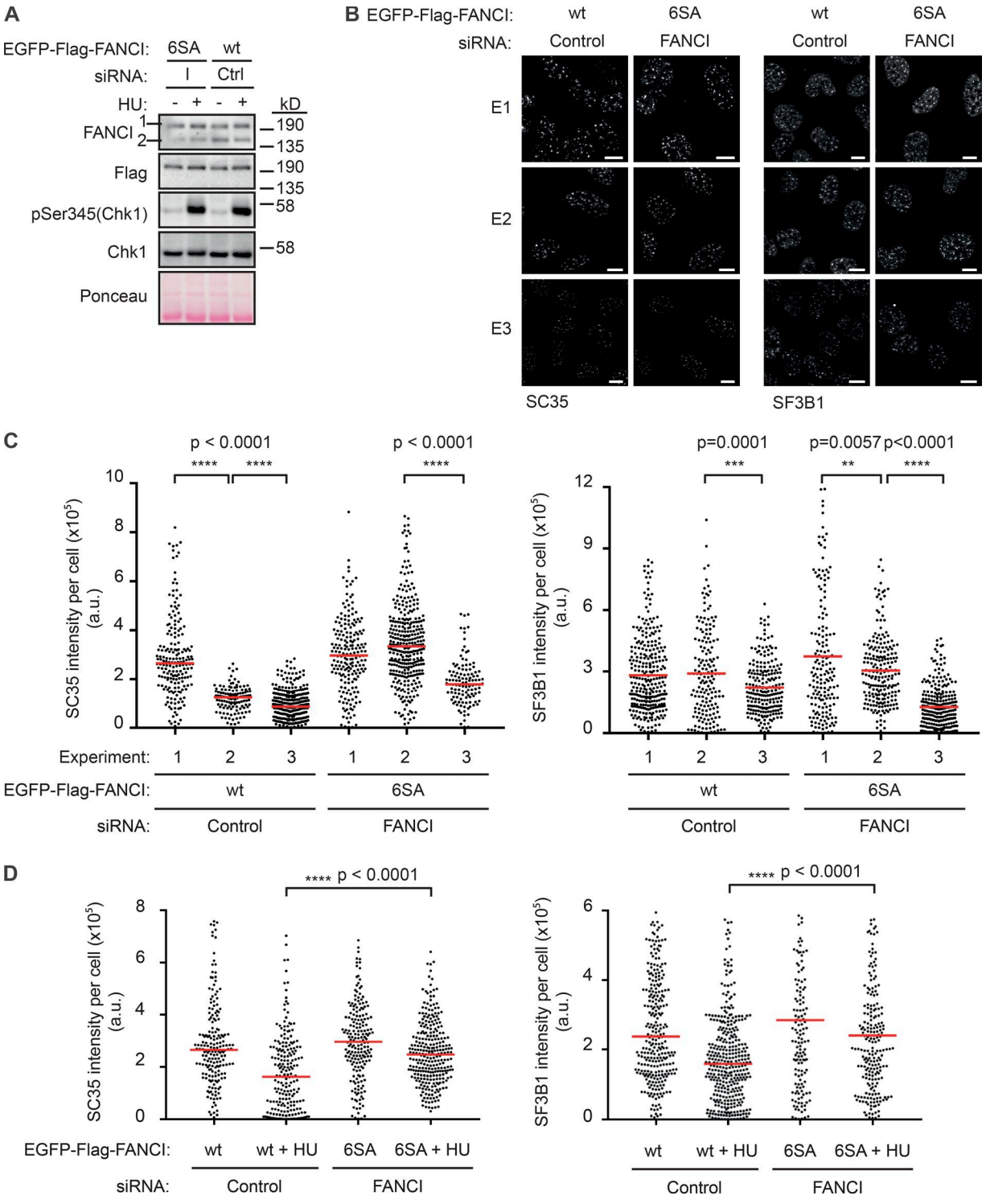

Figure 9. **FANCI-mediated release of SFs from speckles in response to HU is dependent on ATR.** (A) IB of EGFP-Flag-FANCI^{WT} or EGFP-Flag-FANCI^{6SA} (1) and endogenous FANCI (2) in siRNA-transfected U2OS stable cells (Ctrl, siControl; I, siFANCI) treated or not with 5 mM HU for 1 h. (B and C) SC35 and SF3B1 IF in stable U2OS cell lines used in A in three consecutive experiments (marked E1–E3). Representative images of each experiment are shown in B. (C) Quantification as in Fig. 3. (D) Quantification of SC35 and SF3B1 IF in U2OS cell lines used in A treated or not with 5 mM HU for 1 h. Quantification as in Fig. 3. At least 120 cells were quantified per biological replicate. Bars, 10 µm.

whereas FANCD2 depletion yields cellular phenotypes expected from an increase in U2 snRNP levels near pre-mRNAs. In summary, FANCI associates with and regulates the dynamics of the nucleoplasmic pool of SFs, whereas FANCD2 associates with the chromatin-bound pool of SFs (Fig. 10, model).

The FA pathway protects against genome instability induced by interference between transcription and DNA replication (García-Rubio et al., 2015; Schwab et al., 2015). FANCD2 alleviates transcription/DNA replication conflicts at fragile sites independently of its monoubiquitination (Madireddy et

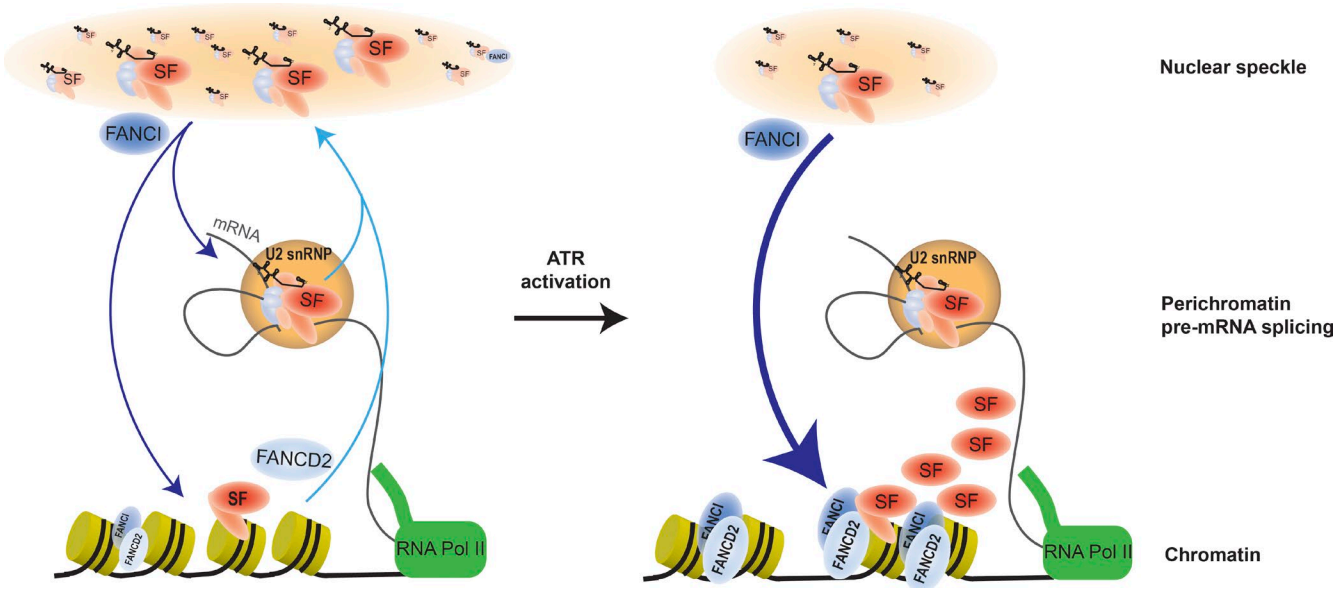

Figure 10. **Model.** FANCI promotes the release of SFs from nuclear speckles to sites of cotranscriptional splicing in perichromatin, whereas FANCD2 facilitates the disassembly of postcatalytic splicing complexes. ATR activation in response to DNA damage induces the accumulation of FANCI and FANCD2 in chromatin and the release of SFs from nuclear speckles in a FANCI-dependent manner. FANCD2 accumulates at DNA damage sites, which may keep it functionally away from postcatalytic spliceosomes. This in turn modifies the organization of functional sites in chromatin and delays the release of postcatalytic SFs under conditions of genotoxic stress.

al., 2016). We show here that FANCD2 and FANCI promote the timely eviction of SFs from condensing chromatin and the removal of postcatalytic intron lariats. The data suggest that coordination of DNA replication and cotranscriptional processes by FANCD2 and FANCI may reflect their function in the organization of functional domains in chromatin.

Changes in the nuclear distribution of SFs can influence cell differentiation and contribute to the pathogenesis of diseases (Saltzman et al., 2011; Dardenne et al., 2012; Wong et al., 2013; Fiszbein et al., 2016). As FA proteins are likely to induce qualitative change in splicing, alterations in the transcriptional repertoire could underlie some clinical features of FA. Consistent with this, the FA pathway determines the expression of the tumor suppressor *TAp63* and of the gene encoding the TGF-β pathway protein SMAD3 (Park et al., 2013; Zhang et al., 2016).

SF3B1 and SC35 are frequently mutated in myelodysplastic syndromes (Visconte et al., 2012). SF3B1 mutations cluster in its solvent-exposed HEAT repeats and do not perturb the association of SF3B1 with other components of the U2 snRNP, or with RNA (Alsafadi et al., 2016; Cretu et al., 2016). FA patients also suffer from myelodysplasia, albeit from a distinct clinical subtype (Tischkowitz and Hodgson, 2003). The findings reported here could have implications for understanding the pathogenesis of FA and cancers associated with mutations in SF3B1.

Materials and methods

Cell culture, plasmids, and chemicals

U2OS, HEK293T, HeLa S3, RPE1-hTERT, and PD20i fibroblasts were grown under standard conditions in DMEM (D5796; Sigma-Aldrich) supplemented with 10% FBS (S181G-500; Biowest) and 1% penicillin-streptomycin (P0781; Sigma-Aldrich). HEK293 cells were grown under standard conditions in RPMI (R8758; Sigma-Aldrich) supplemented with 10% FBS. HEK293 cells stably expressing Flag-tagged FANCI were grown in roller bottles. All experiments were conducted using exponentially growing cells. Cell transfections were performed using INTERFERin (409-50; Polyplus) for siRNAs and Jet-PEI (Qbiogene) for plasmids (along with siRNAs) following the manufacturers' instructions.

Sf21 insect cells were grown in Sf-900 II SFM medium (0902096; Gibco BRL; Fig. 1 B) and ExCell 420 (Sigma-Aldrich; Fig. 1 C). Cells were maintained between 1 and 10 million cells/ml. Flag-FANCI-pCR3 plasmid allowing expression of FANCI tagged with a Flag at its N terminus was a gift from A. D'Andrea and P. Vinciguerra (Dana-Farber Cancer Institute, Boston, MA). Flag-FANCD2 plasmid was obtained by cloning FANCD2 in pCR3. Note that transiently expressed Flag-FANCD2 (48 h) does not localize to chromatin. EGFP-Flag-FANCI^{wt}– and EGFP-Flag-FANCI^{6SA}–expressing plasmids were a gift from T.T. Huang (New York University School of Medicine, New York, NY; Chen et al., 2015). Chemicals used in this study were as follows: HU (H8627; Sigma-Aldrich), ATR inhibitor VE-821 (V134; TINIB Tools), triptolide (PG490; Santa Cruz Biotechnology), MG132 (474790; Calbiochem), aphidicolin (A0781; Sigma-Aldrich), and G418 (A1720; Sigma-Aldrich).

Antibodies

PLA. Rabbit polyclonal antibody against SF3B1 was raised against the peptide NH2-EQYDPFAEHRPPKIAC-COOH (EUROGENTEC) and used at 11 ng/µl; mouse anti-FANCD2 (ab5360; Abcam), 11 ng/µl; mouse anti-FANCI (sc-271316; Santa Cruz Biotechnology), 11 ng/µl; rabbit anti-TFIP11 (A302-548A; Bethyl), 5 ng/µl; rabbit anti-SPF45 (A302-548A; Bethyl), 1 ng/µl; rabbit anti-DHX15 (A300-398AA; Bethyl), 1 ng/µl; anti-rabbit PLUS (DUO92002; Sigma-Aldrich); and anti-mouse MINUS (DUO92004; Sigma-Aldrich).

IB. Antibodies were as follows: rabbit anti-FANCD2 (NB100-182; Novus) at 1:10,000; rabbit anti-FANCI (A301-254A; Bethyl) at 1:1,000; rabbit anti-SF3B1 (A300-996A; Bethyl) at 1:2,000; rabbit anti-SF3B1 (Eurogentec) at 1:1,000; rabbit anti-SF3A3 (A302-507A;

Bethyl) at 1:2,000; rabbit anti-FLAG (F7425; Sigma-Aldrich) at 1:1,000; rabbit anti-DHX15 (A300-389A; Bethyl) at 1:5,000, mouse anti-SC35 (556363; BD Pharmingen) at 1:500; rabbit anti-U2AF65 (ab37530; Abcam) at 1:250; rabbit anti-pSer345(Chk1) (2348L, rabbit; Cell Signaling Technology) at 1:1,000; mouse anti-Chk1 (Sc-8408; Santa Cruz Biotechnology) at 1:1,000; mouse anti-tubulin (T5168; Sigma-Aldrich) at 1:10,000; anti-rabbit HRP-linked (7074; Cell Signaling Technology) at 1:2,500; anti-mouse HRP-linked (7076; Cell Signaling Technology) at 1:2,500; rabbit anti-Nbs1 (NB100-143; Novus Biologicals) at 1:1,000; mouse anti-PCNA (P8825; Sigma-Aldrich) at 1:3,000; rabbit anti-TopBP1 (A300-111A; Bethyl) at 1:1,000; rabbit anti-RNA-PolII (N-20) (sc-899; Santa Cruz Biotechnology) at 1:1,000; rabbit anti-TFIP11 (A302-548A; Bethyl) at 1:1,000; rabbit anti-SPF45 (A302-548A; Bethyl) at 1:1,000; rabbit anti-FANCA (A301-980A; Bethyl) at 1:2,000; and rabbit anti-PRP8 (GTX108046; GeneTex) at 1:1,000.

RNA immunoprecipitation. Antibodies used were as follows: rabbit anti-FANCD2 (NB100-182; Novus), 4 µg per IP; rabbit anti-SF3B1 (A300-996A; Bethyl), 1 µg per IP; rabbit anti-SF3B1 (Eurogentec), 25 µg per IP; rabbit anti-DHX15 (A300-389A; Bethyl), 2 µg per IP; anti-FLAG M2 Affinity Gel (A2220; Sigma-Aldrich), 20 µl per IP; anti-FLAG M2 magnetic beads (M8823; Sigma-Aldrich) 20 µl per IP; and rabbit IgG (NI01; Calbiochem), according amount to be comparable to the experiment.

IF. Antibodies were as follows: mouse anti-SC35 (556363; BD Pharmingen) at 1:300; rabbit anti-SF3B1 (Eurogentec) at 1:200; and Alexa Fluor 546 goat anti–mouse IgG and Alexa Fluor 488 goat anti–rabbit IgG (A11030 and A11008; Invitrogen) at 1:500.

RNA interference

RNA interference was performed using GE Dharmacon siGENOME human siRNA (20 nM): siFANCA (M-019283-02), siFANCD2 (M-016376-02), siFANCI (M-022320-01), siSF3B1 (M-022320-01), and siDHX15 (Dharmacon siRNA target sequence: 5′-GGUUAUAGU UAUGAGCGCUACUCUA-3′), with siGENOME nontargeting siRNA (D-001210-04-20) as control and Qiagen siRNAs (40 nM; FANCI target sequence, 5′-CACGGGCAUCUGGGAGAUAUA-3′; FANCD2 target sequence, 5′-CAACAUACCUCGACUCAUU-3′); SAMHD1 (SI04243673); and CTF18 (SI04347700).

Establishment of Flag-FANCI–expressing HEK293 cells

Flag-FANCI-pCR3 was transfected in HEK293 cells using the calcium phosphate method. HEK293 cells stably expressing Flag-FANCI proteins were selected with G418 (800 µg/ml) and grown under standard conditions.

Establishment of U2OS cell lines overexpressing FANCI^{WT} or FANCI^{6SA}

U2OS cells were transfected with EGFP-Flag-FANCI^{wt}- or FANCI-^{6SA}-containing plasmids using JetPEI (Polyplus) according to the manufacturer's protocol. At 24 h posttransfection, medium was changed, and G418 (700 µg/ml) was added to select transfected cells and generate stable cell lines.

Purification of Flag-FANCI and associated proteins from native chromatin

We used Flag-FANCI HEK293 cells and, as a control, an N-terminal FLAG-BAP Fusion Protein (Sigma-Aldrich) for affinity purification experiments. Native chromatin was prepared from Flag-FANCI HEK293 cells (10^9) exposed to HU (5 mM) for 1 h. Cells were resuspended in sucrose buffer (10 mM Hepes, pH 7.9, 0.34 M sucrose, 3 mM $CaCl_2$, 2 mM magnesium acetate, and 0.1 mM EDTA) containing 0.5% NP-40 and protease inhibitors (PIs; 11836170001, Complete, EDTA-free Protease Inhibitor Cocktail; Roche) and incubated with gentle shaking for 10 min at 4°C. Intact nuclei were pelleted at 3,900 *g* for 20 min, washed with sucrose buffer without NP-40, and resuspended in nucleoplasmic extraction buffer (20 mM Hepes, pH 7.9, 3 mM EDTA, 10% glycerol, 150 mM potassium acetate, and 1.5 mM $MgCl_2$) supplemented with PIs. Extract was homogenized by 20 strokes with a glass homogenizer and incubated with gentle shaking for 20 min at 4°C. The nuclear extract was cleared by centrifugation for 30 min at 14,000 *g* at 4°C. Next, the chromatin-containing pellet was incubated for 1 h at RT in nuclease incubation buffer (150 mM Hepes, pH 7.9, 1.5 mM $MgCl_2$, and 150 mM KOAc) supplemented with PIs and benzonase (125 U/ml) to solubilize chromatin-bound proteins. The native chromatin fraction was cleared by centrifugation at 20,000 *g* for 30 min at 4°C. Next, chromatin extracts were fractionated by gel filtration through HiLoad 16/60 Superdex 200 (GE Healthcare) equilibrated in phosphate buffer P (50 mM Na_2HPO_4/NaH_2PO_4, pH 7.0, 10% glycerol, 0.01% NP-40, 0.5 mM EDTA, and 2 mM tris(2-carboxyethyl)phosphine) supplemented with 150 mM NaCl. Fractions containing Flag-FANCI were pooled and loaded onto a 1-cm^3 M2 agarose (A2220; Sigma-Aldrich) column (Tricorn, GE Healthcare) equilibrated in buffer P supplemented with 150 mM NaCl (buffer P-0.15_{NaCl}). The column was washed with 5 column volumes (CV) of phosphate buffer, and Flag-FANCI was eluted along with associated proteins with 5 CV buffer P-0.15_{NaCl} supplemented with 100 µg/ml 3xFLAG peptide. Eluted proteins were resolved by PAGE, extracted, and identified by liquid chromatography coupled to tandem mass spectrometry. Geneset analysis was performed using STRING (http://string-db.org/).

Protein extract fractionation by ion-exchange, affinity, and size-exclusion chromatography

HEK293 Flag-FANCI cells (packed cell volume of 3 ml) were resuspended in 6 ml buffer P (50 mM Na_2HPO_4/NaH_2PO_4, pH 6.8, 1 mM EDTA, 1 mM DTT, 10% glycerol, and 0.1% NP-40) supplemented with 420 mM NaCl (buffer P-0.42_{NaCl}), and centrifuged twice for 30 min at 16,060 *g*. Soluble protein extract was diluted with buffer P to 0.1 M NaCl, loaded onto a 3-cm^3 phosphocellulose column (Whatman P11) preequilibrated in buffer P-0.1_{NaCl}, washed with 3 CV buffer P-0.1_{NaCl}, and fractionated with a 10-CV gradient to buffer P-1_{NaCl}.

Fractions containing FANCD2, FANCI, and SF3B1 were pooled and loaded onto a preequilibrated 0.6-cm^3 M2 agarose column. Protein elution was achieved using 5 CV buffer P-0.1_{NaCl} supplemented with 100 µg/ml 3xFLAG peptide. Alternatively, 270 µl phosphocellulose pooled fractions were analyzed by gel filtration onto a Superose 6 10/300 GL column (GE Healthcare) in buffer P-0.42_{NaCl}.

Coexpression and purification of Flag-FANCD2–containing complexes

SF3B1 and Flag-FANCD2 cDNAs were optimized for expression in insect and human cells and synthesized by GenScript. SF3B1 was cloned into a pACEBac1 vector and tagged with 6His in its C terminus. Flag-FANCD2 was cloned into a pFastBac1 vector. FANCI was cloned into a pDEST8 vector using Gateway cloning. These constructions were used to express the proteins in a Baculovirus expression system.

For infection, 40 million Sf21 cells (in 20 ml) were infected with baculovirus encoding SF3B1-6His, Flag-FANCD2, and FANCI. After 2 d, infected cells were collected and lysed mechanically using a Dounce (30 strokes) in hypotonic buffer (20 mM Hepes-NaOH, pH 7.5, 5 mM KCl, and 1.5 mM $MgCl_2$) complemented with 1× PIs. Lysate was adjusted to 0.42 M potassium acetate then clarified by centrifugation (43,000 *g*, 30 min, 4°C). Clarified lysate was loaded on a 1-cm^3 M2 agarose column equilibrated with 5 CV FEQ buffer (20 mM Hepes-NaOH, pH 7.5, 0.42 M potassium acetate, 5 mM KCl, and 1.5 mM

$MgCl_2$). Once lysate was injected, the column was washed with 10 CV FW buffer (20 mM Hepes-NaOH, pH 7.5, 0.42 M potassium acetate, 1 mM EDTA, 0.01% Nonidet P-40, and 10% [vol/vol] glycerol, supplemented with 1× PIs). Then elution was done in Q buffer (FW buffer supplemented with 0.15 M potassium acetate and 0.1 mg/ml 3xFLAG peptide; Sigma-Aldrich). 0.5-ml elution fractions were collected using Fractionator 960.

Standard protein extraction

Whole-cell extracts were prepared using high salt buffer (50 mM Tris, pH 7.5, 300 mM NaCl, 1% Triton X-100, and 1 mM DTT) supplemented with PIs. Typically, 1 mg pelleted cells was washed with ice-cold 1× PBS, resuspended in 300 µl high salt buffer, vortexed vigorously, and centrifuged for 30 min at 16,060 *g*, 4°C. Supernatants were recovered and subjected again to the same clearing process. To prepare chromatin extracts, we followed the procedure described in the Purification of Flag-FANCI and associated proteins from native chromatin section.

PLAs

We used the Duolink In Situ kit (DUO92014; Sigma-Aldrich) according to the manufacturer's instructions. U2OS cells were fixed onto 1-cm-diameter slides using 2% PFA and 2% sucrose for 20 min at RT. Where indicated, the soluble fraction of cells was eliminated by a preextraction step (2 × 3 min) in CSK buffer (10 mM Pipes, pH 7, 100 mM NaCl, 300 mM sucrose, 3 mM $MgCl_2$, and 0.7% Triton X-100), and total RNA was digested using RNase A (0.3 µg/ml, R4875; Sigma-Aldrich). The slides were incubated in 1× PBS + 0.1% Tween + 0.2% Triton X-100 for 10 min, and then washed three times in 1× PBS. Next, the slides were saturated with 1× PBS + 2% BSA + 0.05% Tween for 1 h at RT. Each slide was then incubated on top of a layer of PBS-Tween containing the primary antibody in a humid chamber at 4°C overnight. The next day, the slides were washed three times with 1× PBS. Secondary antibodies coupled to the DNA probes (DNA probe rabbit, DUO92002; DNA probe mouse, DUO092004) were mixed together as indicated by the manufacturer (one-fifth of each probe + three-fifths of blocking reagent included in the kit) for 20 min at RT. Incubation with the mix of secondary antibodies was performed in a humid chamber for 1 h at 37°C. Slides were subsequently washed twice for 5 min with buffer A (150 mM NaCl, 10 mM Tris-Base, and 0.5% Tween 20, pH 7.4) before incubation with 20 µl ligation mix for 30 min at 37.0°C. Next, the slides were washed twice for 2 min with buffer A before incubation with 20 µl amplification mix for 100 min at 37°C in the humid chamber. The slides were washed twice for 10 min in buffer B (200 mM NaCl and 400 mM Tris-Base, pH 7.5) and then briefly in water before embedding the slides with DAPI DNA staining and PLA signal preserving mounting medium (DUO82040; Sigma-Aldrich). PLA signals were visualized by fluorescent microscopy using light-exciting FITC and acquired via a Coolsnap HQ Camera from a Leica DM6000 microscope using a 40× PL APO 1.25 oil or 63× PL APO 1.4 oil objective lens and Metamorph acquisition software. Fig. 1 F was acquired via a Zeiss CCD Axiocam Mrm monochrome from a Zeiss AxioImager Z1 microscope using a 25× Plan Neofluar 0.8-NA Imm Korr objective lens and Zen software. Images were acquired at 20°C–23°C. Image mounting was done using Omero (University of Dundee and Open Microscopy Environment).

Quantification of PLA and IF signals

All the individual signals of a nucleus were recorded for each nucleus using an ImageJ macro (signals in nuclei.ijm, see the supplemental ZIP file). Next, the data were exported to an Excel table in .csv file format. This file was subjected to a script in Galaxy (https://usegalaxy.org) that adds up all values belonging to a single nucleus to obtain the total signal per nucleus. The workflow can be accessed by typing "intensity-per-nucleus" in the "published workflows" section of Galaxy, or directly uploading the command file ("Galaxy-Workflow-Intensity-per-nucleus_IFs-quantification.ga," see Text S1 in the supplemental material). Final values were plotted using GraphPad Prism.

IF

For SC35 speckle detection, U2OS cells were fixed with 2% PFA onto 1-cm-diameter slides and permeabilized with 1× PBS + 0.1% Tween 20 + 0.2% Triton X-100 for 10 min at RT; for SF3B1-speckles, or double staining SC35/SF3B1, the fixation was performed with cold methanol for 8 min, followed by rehydration with PBS for 5 min before the permeabilization step. Where indicated, soluble proteins were preextracted using CSK buffer before fixation to leave only proteins strongly attached to the chromatin. After fixation by any of these methods, each slide was incubated with 1× PBS + 0.1% Tween 20 + 5% BSA containing the primary antibodies in a humid chamber at RT for 90 min and washed three times for 10 min in 1× PBS + 0.1% Tween 20. Secondary antibodies were incubated for 45 min in a humid chamber and darkness at RT and washed three times for 10 min in 1× PBS + 0.1% Tween 20 in darkness. DNA dye Hoechst was included in the final wash. Brief washing with water was performed before mounting with ProLong Antifade Reagent (P36930; Life Technologies). IF signals were detected using adequate fluorochromes according to antibodies listed in the Antibodies section and acquired via a Zeiss CCD Axiocam Mrm monochrome from a Zeiss AxioImager Z1 microscope with ApoTome technology (Zeiss; see next section for additional information) using a 40× Plan Apochromat 1.3-NA oil or 63× Plan Apochromat 1.4-NA oil objective lens and Zen software. Images were acquired at 20°C–23°C. Image mounting was done using OMERO (open microscopy environment).

Image acquisition by ApoTome and optical sectioning using structured illumination

Quantification of speckle intensity was performed using ApoTome-acquired images. ApoTome technology allows the acquisition of optical sections free of scattered light to analyze one focal plane. Optical sectioning allows higher resolution than wide-field microscopy, providing well-defined and reliably quantifiable images of speckles. The advantages of these images are that the signal coming from diffuse and chromatin-bound protein is distinguishable from that of speckles, and the scattered out-of-focus light around them is removed (Fig. 3 A, compare Apo vs. No Apo). The intensity of speckles per cell was automatically quantified using an ImageJ macro available in the online supplemental material.

Preparation of circular RNA

Total RNA (2 µg) was prepared using the GenElute Mammalian Total RNA Miniprep kit (RTN70; Sigma-Aldrich). Half of the preparation was digested with 2 U RNase R (RNR07250; Epicentre), or none as control, in 1× RNase R reaction buffer for 15 min at 37°C. Samples were resolved by agarose (0.8%) gel electrophoresis and visualized with GelRed. GelRed, and not ethidium bromide, is crucial for accurate migration of the samples.

Northern blotting

Agarose gels were first treated with 50 mM NaOH and 10 mM NaCl for 20 min, and then with 10 mM Tris-HCl, pH 7.5, for 20 min. The gels were equilibrated in 20× SSC (3 M NaCl and 0.3 M Na_3Citrate.$2H_2O$, pH 7) for at least 30 min. Transfer to a Hybond XL membrane (RPN303S; GE Healthcare) was achieved by capillarity. Nucleic acids were fixed to the membrane by UV-irradiating each side with 70,000 µJ/cm^2. For hybridization, membranes were equilibrated for at least 1 h at 65°C in 0.5 M $NaPO_4$, pH 7, and 7% SDS. The probe to detect linear GAPDH

was designed to target exon 5. It was PCR-amplified from retrotranscribed RNA using the following primers: forward, 5′-ATTTGGTCG TATTGGGCG-3′, and reverse, 5′-AGTTGAGGTCAATGAAGGG-3′. The probe was labeled by random priming, purified by means of MicroSpin G-50 columns (27-5330-01; GE Healthcare), heat-denatured, and added to the same solution. Incubations were performed overnight in a rotating oven at 65°C. The next morning, we performed three washes with 0.1× SSPE, 5 mM EDTA, pH 8, and 0.5% SDS at 65°C for at least 1 h. Radioactive signals were captured using a Fujifilm imaging plate and visualized using a Typhoon TRIO+ (Amersham).

Retrotranscription

Retrotranscription reactions (20 µl) were performed using random primers on total RNA (500 ng) extracted using the GenElute Mammalian Total RNA Miniprep kit (RTN70; Sigma-Aldrich) or on immunoprecipitated RNA (1–10 µl of final product). In both cases, we used the SuperScript III reverse transcription kit from Invitrogen and followed the manufacturer's indications. Alternative splicing events were scored using the following primers: FAM62B (forward, 5′-GTG CTAACAGACATCAAAGCTGA-3′; reverse, 5′-CCCAACTGACAT CTGGACAA); FIP1L1 (forward, 5′-GAGGATACGAATGGGACT TGA-3′; reverse, 5′-TGGAAGCCCAGTCTTGAACA); ECHDC1 (forward, 5′-AGAGGGGAAAGGCCTCATT-3′; reverse, 5′-ATT CTGCTCCTCCACCCAAT); PSMG1 (forward, 5′-GTCTGGGAG GAAGTTGGTTG-3′; reverse, 5′-TGCATGTTCTTCCTTGGACA; RAC1 (forward, 5′-GGTAGATGGAAAACCGGTGA-3′; reverse, 5′-CTTTGCACGGACATTTTCAA); MACF1(forward, 5′-CCTACT CGTTCCAGCTCCAG-3′; reverse, 5′-AAGTCAGAAGCGTCACTT CC); STARD3NL (forward, 5′-CTTCTGGCAGTTTTTCGATTT-3′; reverse, 5′-CAGGAACCACGTCTCAATCC; DAB2 (forward, 5′-AATGGGAGTGAGGCCCTAAT-3′; reverse, 5′-CGTTGGTCGAGG AAGAGAAC); HHLA3 (forward, 5′-CAGACCCCAAGAGAGCAT TC-3′; reverse, 5′-GGGCAGGAACAAATCACAAT); ABI2 (forward, 5′-GCCATACTCCCCCAACAATA-3′; reverse, 5′-GTGGGG GAGACTCATCAAAG); ATXN2 (forward, 5′-CAACTCAGTACG GGGCTCAT-3′; reverse, 5′-GACTGGGTGCAGGATGACTT); and MAP3K7 (forward, 5′-CTCCATCCCAATGGCTTATC-3′; reverse, 5′-TTTTTGCATTGCTGGTAGTAAG).

Evaluation of FANCI and FANCD2 mRNA levels was done with the following primers: FANCI (forward, 5′-GGGGACAAGTTT GTACAAAAAAGCAGGCCTCGCCACCATGGACCAGAAGATTTT ATCTC-3′; reverse, 5′-GGGGACCACTTTGTACAAGAAAGCTGG GTCTTATTTTTTCCTTTTCTTCTTG); FANCD2 (forward, 5′-GGG GACAAGTTTGTACAAAAAAGCAGGCTTCGCCACCATGGTTTC CAAAAGAAGACTG-3′; reverse, 5′-GGGGACCACTTTGTACAA GAAAGCTGGGTCCTAATCAGAGTCATCATAACTCTCA); U2 (forward, 5′-ATCGCTTCTCGGCCTTTTGGC-3′; reverse, 5′-TGG TGCACCGTTCCTGGAGG); and Tyr tRNA (forward, 5′-CCTTCG ATAGCTCAGCTGGTAGAGCGGAGG-3′; reverse, 5′-CGGAATTGA ACCAGCGACCTAAGGATGTCC).

RNA immunoprecipitation

All manipulations were performed using filter tips. Typically, 5×10^6 cells were seeded on 140-mm-diameter plates the day before the preparation of chromatin extract (yielding up to 300 µg total proteins). The cells were cross-linked with 1% formaldehyde for 10 min under agitation at RT, and formaldehyde was quenched using 125 mM glycine for 15 min. Cells were washed twice with cold 1× PBS supplemented with PIs and collected by centrifugation at 137 *g* for 5 min at 4°C. The pellet was resuspended in 5 ml wash I buffer (0.25% Triton X-100, 10 mM EDTA, 0.5 mM EGTA, and 10 mM Hepes) supplemented with PIs for 10 min at 4°C, then centrifuged at 137 *g* for 5 min at 4°C. The pellet was subsequently resuspended in 5 ml wash II buffer (200 mM NaCl, 1 mM EDTA, 0.5 mM EGTA, and 10 mM Hepes) supplemented with PIs for 10 min at 4°C, centrifuged for 5 min at 4°C at 137 *g*, and resuspended and incubated in 1 volume lysis buffer (1% SDS, 10 mM EDTA, and 50 mM Tris, pH 8) freshly supplemented with PIs and 40 units RNasin (N2511; Promega) per milliliter of buffer for 30 min at 4°C. Chromatin extracts (300-µl aliquots) were sonicated using Bioruptor (Diagenode), alternating 30 s ON/30 s OFF, power high during 10 min. Next, extracts were incubated for 30 min at 37°C with DNase I (30 units; Z358A; Promega) in 1× DNase I buffer and sonicated again similarly. Debris was removed by centrifugation at 18,620 *g* for 5 min at 4°C, and the clarified supernatant was recovered. The efficiency of sonication was assessed via 1% agarose gel electrophoresis. 10% of this material was saved to probe the input. The remaining material was split into three samples, and volume was taken up to 1 mL with dilution buffer (0.01% SDS, 1.1% Triton X-100, 1.2 mM EDTA, 16.7 mM Tris, pH 8, 167 mM NaCl, and RNasin added for RNA-IPs) and incubated overnight with anti-SF3B1, anti-FANCD2, and anti-IgG antibodies on a rotating wheel at 4°C. Immunoprecipitations were performed during the course of a 2-h incubation at 4°C using 12 µl Protein A Magnetic Beads (10001D; Life Technologies) equilibrated in dilution buffer and saturated with 1 mg/ml BSA. Next, the supernatant was discarded, and the beads were washed for 10 min at 4°C with 700 µl RIPA buffer (150 mM NaCl, 50 mM Tris, pH 8, 0.1% SDS, 0.5% NaDoc, and 1% NP-40) supplemented with RNAsin, followed by high salt buffer (500 mM NaCl, 50 mM Tris, pH 8, 0.1% SDS, and 1% NP-40) supplemented with RNAsin, LiCl buffer (250 mM LiCl, 50 mM Tris, pH 8, 0.5% NaDoc, and 1% NP-40) supplemented with RNAsin, and finally 1× TE buffer (10 mM Tris, pH 8, and 1 mM EDTA) supplemented with 100 mM NaCl.

The immunoprecipitated material was mixed gently with 75 µl chromatin immunoprecipitation elution buffer (100 mM Tris-Cl, pH 8, 10 mM EDTA, and 1% [wt/vol] SDS) supplemented with RNAsin and eluted during the course of a 10-min incubation at 37°C in a water bath. Eluted material was recovered in the supernatant after centrifugation at 5,040 *g* for 2 min at RT. The elution procedure was repeated once, and the eluates were pooled. 30 µl was saved for IB. The remaining 120 µl per condition was brought to a final concentration of 200 mM NaCl. Proteins were digested for 1 h at 42°C using proteinase K (20 µg). Next, formaldehyde cross-links were reversed for 1 h at 65°C.

The RNA preparation was completed to 250 µl with nuclease-free water, extracted with phenol/chloroform, (5:1, acid equilibrated at pH 4.7), ethanol-precipitated, and resuspended in 200 µl TE buffer, pH 7.5. 2-µl aliquots were retrotranscribed (20 µl reactions), and one-fifth of the RT reaction was used for PCR amplification. The following primers were used for retrotranscription: U2 (forward, 5′-ATCGCTTCTCGGCCTTTTGGC-3′; reverse, 5′-TGGTGC ACCGTTCCTGGAGG) and Tyr tRNA (forward, 5′-CCTTCGATA GCTCAGCTGGTAGAGCGGAGG-3′; reverse, 5′-CGGAATTGA ACCAGCGACCTAAGGATGTCC).

Standard immunoprecipitations

Protein extracts were prepared as indicated in the Standard protein extraction section. Approximately 600 µg protein was used per immunoprecipitation. Anti-Flag M2-affinity gel (A2220; Sigma-Aldrich) was used to pull down Flag-tagged proteins by incubation with protein extract overnight at 4°C. Protein A/G Dynabeads (10001D/10004D; Life Technologies) were used to immunoprecipitate endogenous proteins. For endogenous protein immunoprecipitation from HEK293 cells, chromatin extracts in native conditions were prepared as described in the Purification of Flag-FANCI and associated proteins from native chromatin section. The chromatin fractions were incubated overnight

with 1 µg/ml of the corresponding antibody. Simultaneously, Dynabeads were saturated with 20 mg/ml BSA. Dynabeads were washed twice with nuclease incubation buffer (150 mM Hepes, pH 7.9, 1.5 mM $MgCl_2$, and 150 mM KOAc) supplemented with PIs before incubation with protein extract for 2 h at 4°C. Immunoprecipitates were washed extensively, resuspended in protein sample loading buffer, boiled for 5 min, and analyzed by Western blotting.

Online supplemental material

Fig. S1 shows functional enrichment of proteins associated with FANCI and the impact of SF3B1 depletion on the expression of DDR proteins. The corresponding mass spectrometry table is available in the JCB DataViewer at https://doi.org/10.1083/jcb.201702136.dv. Fig. S2 shows the localization of FA proteins and of SFs in mitotic cells. Fig. S3 shows additional controls experiments related to Fig. 4. Fig. S4 shows replicates of experiments presented in Fig. 6. Fig. S5 shows additional controls and replicates of experiments presented in Figs. 6 and 7. Two custom algorithms (nuclei.ijm and Galaxy-Workflow-Intensity-per-nucleus_IFs-quantification.ga) are included to quantify IF signals as described in Materials and methods.

Acknowledgments

We thank M. Delannoy and P. Bertrand for technical help; A. D'Andrea, T. Huang, F. Rosselli, and Y-L. Lin for reagents; R.F. de Luco, M-H. Stern, R. Kiernan, A. Aguilera, C. Ribeyre, and J. Basbous for suggestions and critical reading; the Montpellier Rio Imaging facility; J. Cau and R. Forey for providing tools for IF quantification; and P. Pasero and B. Pardo for support.

Fondation ARC pour la Recherche sur le Cancer (CT060509), Institut National du Cancer (2015-1-PL BIO-03), and MSD Avenir (GnoStiC) supported this work. S. Ovejero is the recipient of a fellowship from Ligue Contre le Cancer.

The authors declare no competing financial interests.

Author contributions: M. Moriel-Carretero, S. Ovejero, and M. Gérus-Durand: conceptualization, data curation, investigation, methodology, and writing. D. Vryzas: investigation. A. Constantinou: conceptualization, funding acquisition, supervision, validation, writing, review, and editing.

Submitted: 22 February 2017
Revised: 2 August 2017
Accepted: 25 August 2017

References

Adamson, B., A. Smogorzewska, F.D. Sigoillot, R.W. King, and S.J. Elledge. 2012. A genome-wide homologous recombination screen identifies the RNA-binding protein RBMX as a component of the DNA-damage response. *Nat. Cell Biol.* 14:318–328. https://doi.org/10.1038/ncb2426

Agafonov, D.E., J. Deckert, E. Wolf, P. Odenwälder, S. Bessonov, C.L. Will, H. Urlaub, and R. Lührmann. 2011. Semiquantitative proteomic analysis of the human spliceosome via a novel two-dimensional gel electrophoresis method. *Mol. Cell. Biol.* 31:2667–2682. https://doi.org/10.1128/MCB.05266-11

Alsafadi, S., A. Houy, A. Battistella, T. Popova, M. Wassef, E. Henry, F. Tirode, A. Constantinou, S. Piperno-Neumann, S. Roman-Roman, et al. 2016. Cancer-associated SF3B1 mutations affect alternative splicing by promoting alternative branchpoint usage. *Nat. Commun.* 7:10615. https://doi.org/10.1038/ncomms10615

Beyer, A.L., and Y.N. Osheim. 1988. Splice site selection, rate of splicing, and alternative splicing on nascent transcripts. *Genes Dev.* 2:754–765. https://doi.org/10.1101/gad.2.6.754

Castella, M., C. Jacquemont, E.L. Thompson, J.E. Yeo, R.S. Cheung, J.W. Huang, A. Sobeck, E.A. Hendrickson, and T. Taniguchi. 2015. FANCI regulates recruitment of the FA core complex at sites of DNA damage independently of FANCD2. *PLoS Genet.* 11:e1005563. https://doi.org/10.1371/journal.pgen.1005563

Ceccaldi, R., K. Parmar, E. Mouly, M. Delord, J.M. Kim, M. Regairaz, M. Pla, N. Vasquez, Q.S. Zhang, C. Pondarre, et al. 2012. Bone marrow failure in Fanconi anemia is triggered by an exacerbated p53/p21 DNA damage response that impairs hematopoietic stem and progenitor cells. *Cell Stem Cell.* 11:36–49. https://doi.org/10.1016/j.stem.2012.05.013

Ceccaldi, R., P. Sarangi, and A.D. D'Andrea. 2016. The Fanconi anaemia pathway: New players and new functions. *Nat. Rev. Mol. Cell Biol.* 17:337–349. https://doi.org/10.1038/nrm.2016.48

Chen, Y.H., M.J. Jones, Y. Yin, S.B. Crist, L. Colnaghi, R.J. Sims III, E. Rothenberg, P.V. Jallepalli, and T.T. Huang. 2015. ATR-mediated phosphorylation of FANCI regulates dormant origin firing in response to replication stress. *Mol. Cell.* 58:323–338. https://doi.org/10.1016/j.molcel.2015.02.031

Corrionero, A., B. Miñana, and J. Valcárcel. 2011. Reduced fidelity of branch point recognition and alternative splicing induced by the anti-tumor drug spliceostatin A. *Genes Dev.* 25:445–459. https://doi.org/10.1101/gad.2014311

Cretu, C., J. Schmitzová, A. Ponce-Salvatierra, O. Dybkov, E.I. De Laurentiis, K. Sharma, C.L. Will, H. Urlaub, R. Lührmann, and V. Pena. 2016. Molecular architecture of SF3b and structural consequences of its cancer-related mutations. *Mol. Cell.* 64:307–319. https://doi.org/10.1016/j.molcel.2016.08.036

Dardenne, E., S. Pierredon, K. Driouch, L. Gratadou, M. Lacroix-Triki, M.P. Espinoza, E. Zonta, S. Germann, H. Mortada, J.P. Villemin, et al. 2012. Splicing switch of an epigenetic regulator by RNA helicases promotes tumor-cell invasiveness. *Nat. Struct. Mol. Biol.* 19:1139–1146. https://doi.org/10.1038/nsmb.2390

Deans, A.J., and S.C. West. 2009. FANCM connects the genome instability disorders Bloom's syndrome and Fanconi anemia. *Mol. Cell.* 36:943–953. https://doi.org/10.1016/j.molcel.2009.12.006

Dufour, C., A. Corcione, J. Svahn, R. Haupt, V. Poggi, A.N. Béka'ssy, R. Scimè, A. Pistorio, and V. Pistoia. 2003. TNF-alpha and IFN-gamma are overexpressed in the bone marrow of Fanconi anemia patients and TNF-alpha suppresses erythropoiesis in vitro. *Blood.* 102:2053–2059. https://doi.org/10.1182/blood-2003-01-0114

Feric, M., N. Vaidya, T.S. Harmon, D.M. Mitrea, L. Zhu, T.M. Richardson, R.W. Kriwacki, R.V. Pappu, and C.P. Brangwynne. 2016. Coexisting liquid phases underlie nucleolar subcompartments. *Cell.* 165:1686–1697. https://doi.org/10.1016/j.cell.2016.04.047

Fiszbein, A., L.E. Giono, A. Quaglino, B.G. Berardino, L. Sigaut, C. von Bilderling, I.E. Schor, J.H. Steinberg, M. Rossi, L.I. Pietrasanta, et al. 2016. Alternative splicing of G9a regulates neuronal differentiation. *Cell Reports.* 14:2797–2808. https://doi.org/10.1016/j.celrep.2016.02.063

Fourmann, J.B., J. Schmitzová, H. Christian, H. Urlaub, R. Ficner, K.L. Boon, P. Fabrizio, and R. Lührmann. 2013. Dissection of the factor requirements for spliceosome disassembly and the elucidation of its dissociation products using a purified splicing system. *Genes Dev.* 27:413–428. https://doi.org/10.1101/gad.207779.112

Fourmann, J.B., O. Dybkov, D.E. Agafonov, M.J. Tauchert, H. Urlaub, R. Ficner, P. Fabrizio, and R. Lührmann. 2016. The target of the DEAH-box NTP triphosphatase Prp43 in Saccharomyces cerevisiae spliceosomes is the U2 snRNP-intron interaction. *eLife.* 5:e15564. https://doi.org/10.7554/eLife.15564

Garaycoechea, J.I., G.P. Crossan, F. Langevin, M. Daly, M.J. Arends, and K.J. Patel. 2012. Genotoxic consequences of endogenous aldehydes on mouse haematopoietic stem cell function. *Nature.* 489:571–575. https://doi.org/10.1038/nature11368

Garcia-Higuera, I., T. Taniguchi, S. Ganesan, M.S. Meyn, C. Timmers, J. Hejna, M. Grompe, and A.D. D'Andrea. 2001. Interaction of the Fanconi anemia proteins and BRCA1 in a common pathway. *Mol. Cell.* 7:249–262. https://doi.org/10.1016/S1097-2765(01)00173-3

García-Rubio, M.L., C. Pérez-Calero, S.I. Barroso, E. Tumini, E. Herrera-Moyano, I.V. Rosado, and A. Aguilera. 2015. The Fanconi anemia pathway protects genome integrity from R-loops. *PLoS Genet.* 11:e1005674. https://doi.org/10.1371/journal.pgen.1005674

Girard, C., C.L. Will, J. Peng, E.M. Makarov, B. Kastner, I. Lemm, H. Urlaub, K. Hartmuth, and R. Lührmann. 2012. Post-transcriptional spliceosomes are retained in nuclear speckles until splicing completion. *Nat. Commun.* 3:994. https://doi.org/10.1038/ncomms1998

Gozani, O., J. Potashkin, and R. Reed. 1998. A potential role for U2AF-SAP 155 interactions in recruiting U2 snRNP to the branch site. *Mol. Cell. Biol.* 18:4752–4760. https://doi.org/10.1128/MCB.18.8.4752

Haneline, L.S., H.E. Broxmeyer, S. Cooper, G. Hangoc, M. Carreau, M. Buchwald, and D.W. Clapp. 1998. Multiple inhibitory cytokines induce deregulated progenitor growth and apoptosis in hematopoietic cells from Fac-/- mice. *Blood.* 91:4092–4098.

Ishiai, M., H. Kitao, A. Smogorzewska, J. Tomida, A. Kinomura, E. Uchida, A. Saberi, E. Kinoshita, E. Kinoshita-Kikuta, T. Koike, et al. 2008. FANCI phosphorylation functions as a molecular switch to turn on the Fanconi anemia pathway. *Nat. Struct. Mol. Biol.* 15:1138–1146. https://doi.org/10.1038/nsmb.1504

Johnson, T.C., and J.J. Holland. 1965. Ribonucleic acid and protein synthesis in mitotic HeLa cells. *J. Cell Biol.* 27:565–574. https://doi.org/10.1083/jcb.27.3.565

Joo, W., G. Xu, N.S. Persky, A. Smogorzewska, D.G. Rudge, O. Buzovetsky, S.J. Elledge, and N.P. Pavletich. 2011. Structure of the FANCI-FANCD2 complex: Insights into the Fanconi anemia DNA repair pathway. *Science.* 333:312–316. https://doi.org/10.1126/science.1205805

Kee, Y., and A.D. D'Andrea. 2012. Molecular pathogenesis and clinical management of Fanconi anemia. *J. Clin. Invest.* 122:3799–3806. https://doi.org/10.1172/JCI58321

Kfir, N., G. Lev-Maor, O. Glaich, A. Alajem, A. Datta, S.K. Sze, E. Meshorer, and G. Ast. 2015. SF3B1 association with chromatin determines splicing outcomes. *Cell Reports.* 11:618–629. https://doi.org/10.1016/j.celrep.2015.03.048

Knipscheer, P., M. Räschle, A. Smogorzewska, M. Enoiu, T.V. Ho, O.D. Schärer, S.J. Elledge, and J.C. Walter. 2009. The Fanconi anemia pathway promotes replication-dependent DNA interstrand cross-link repair. *Science.* 326:1698–1701. https://doi.org/10.1126/science.1182372

Kottemann, M.C., and A. Smogorzewska. 2013. Fanconi anaemia and the repair of Watson and Crick DNA crosslinks. *Nature.* 493:356–363. https://doi.org/10.1038/nature11863

Kwon, I., S. Xiang, M. Kato, L. Wu, P. Theodoropoulos, T. Wang, J. Kim, J. Yun, Y. Xie, and S.L. McKnight. 2014. Poly-dipeptides encoded by the C9orf72 repeats bind nucleoli, impede RNA biogenesis, and kill cells. *Science.* 345:1139–1145. https://doi.org/10.1126/science.1254917

Laguette, N., C. Brégnard, P. Hue, J. Basbous, A. Yatim, M. Larroque, F. Kirchhoff, A. Constantinou, B. Sobhian, and M. Benkirane. 2014. Premature activation of the SLX4 complex by Vpr promotes G2/M arrest and escape from innate immune sensing. *Cell.* 156:134–145. https://doi.org/10.1016/j.cell.2013.12.011

Lamond, A.I., and D.L. Spector. 2003. Nuclear speckles: A model for nuclear organelles. *Nat. Rev. Mol. Cell Biol.* 4:605–612. https://doi.org/10.1038/nrm1172

Lossaint, G., M. Larroque, C. Ribeyre, N. Bec, C. Larroque, C. Décaillet, K. Gari, and A. Constantinou. 2013. FANCD2 binds MCM proteins and controls replisome function upon activation of S phase checkpoint signaling. *Mol. Cell.* 51:678–690. https://doi.org/10.1016/j.molcel.2013.07.023

Madireddy, A., S.T. Kosiyatrakul, R.A. Boisvert, E. Herrera-Moyano, M.L. García-Rubio, J. Gerhardt, E.A. Vuono, N. Owen, Z. Yan, S. Olson, et al. 2016. FANCD2 facilitates replication through common fragile sites. *Mol. Cell.* 64:388–404. https://doi.org/10.1016/j.molcel.2016.09.017

Marzahn, M.R., S. Marada, J. Lee, A. Nourse, S. Kenrick, H. Zhao, G. Ben-Nissan, R.M. Kolaitis, J.L. Peters, S. Pounds, et al. 2016. Higher-order oligomerization promotes localization of SPOP to liquid nuclear speckles. *EMBO J.* 35:1254–1275. https://doi.org/10.15252/embj.201593169

Mayas, R.M., H. Maita, D.R. Semlow, and J.P. Staley. 2010. Spliceosome discards intermediates via the DEAH box ATPase Prp43p. *Proc. Natl. Acad. Sci. USA.* 107:10020–10025. https://doi.org/10.1073/pnas.0906022107

Meetei, A.R., Z. Yan, and W. Wang. 2004. FANCL replaces BRCA1 as the likely ubiquitin ligase responsible for FANCD2 monoubiquitination. *Cell Cycle.* 3:179–181. https://doi.org/10.4161/cc.3.2.656

Misteli, T., J.F. Cáceres, and D.L. Spector. 1997. The dynamics of a pre-mRNA splicing factor in living cells. *Nature.* 387:523–527. https://doi.org/10.1038/387523a0

Oka, Y., S. Bekker-Jensen, and N. Mailand. 2015. Ubiquitin-like protein UBL5 promotes the functional integrity of the Fanconi anemia pathway. *EMBO J.* 34:1385–1398. https://doi.org/10.15252/embj.201490376

Panneerselvam, J., A. Pickering, B. Han, L. Li, J. Zheng, J. Zhang, Y. Zhang, and P. Fei. 2014. Basal level of FANCD2 monoubiquitination is required for the maintenance of a sufficient number of licensed-replication origins to fire at a normal rate. *Oncotarget.* 5:1326–1337. https://doi.org/10.18632/oncotarget.1796

Park, E., H. Kim, J.M. Kim, B. Primack, S. Vidal-Cardenas, Y. Xu, B.D. Price, A.A. Mills, and A.D. D'Andrea. 2013. FANCD2 activates transcription of TAp63 and suppresses tumorigenesis. *Mol. Cell.* 50:908–918. https://doi.org/10.1016/j.molcel.2013.05.017

Pederiva, C., S. Böhm, A. Julner, and M. Farnebo. 2016. Splicing controls the ubiquitin response during DNA double-strand break repair. *Cell Death Differ.* 23:1648–1657. https://doi.org/10.1038/cdd.2016.58

Räschle, M., P. Knipscheer, M. Enoiu, T. Angelov, J. Sun, J.D. Griffith, T.E. Ellenberger, O.D. Schärer, and J.C. Walter. 2008. Mechanism of replication-coupled DNA interstrand crosslink repair. *Cell.* 134:969–980. https://doi.org/10.1016/j.cell.2008.08.030

Rickman, K.A., F.P. Lach, A. Abhyankar, F.X. Donovan, E.M. Sanborn, J.A. Kennedy, C. Sougnez, S.B. Gabriel, O. Elemento, S.C. Chandrasekharappa, et al. 2015. Deficiency of UBE2T, the E2 ubiquitin ligase necessary for FANCD2 and FANCI ubiquitination, causes FA-T subtype of Fanconi anemia. *Cell Reports.* 12:35–41. https://doi.org/10.1016/j.celrep.2015.06.014

Sacco-Bubulya, P., and D.L. Spector. 2002. Disassembly of interchromatin granule clusters alters the coordination of transcription and pre-mRNA splicing. *J. Cell Biol.* 156:425–436. https://doi.org/10.1083/jcb.200107017

Saltzman, A.L., Q. Pan, and B.J. Blencowe. 2011. Regulation of alternative splicing by the core spliceosomal machinery. *Genes Dev.* 25:373–384. https://doi.org/10.1101/gad.2004811

Sareen, A., I. Chaudhury, N. Adams, and A. Sobeck. 2012. Fanconi anemia proteins FANCD2 and FANCI exhibit different DNA damage responses during S-phase. *Nucleic Acids Res.* 40:8425–8439. https://doi.org/10.1093/nar/gks638

Sato, K., M. Ishiai, K. Toda, S. Furukoshi, A. Osakabe, H. Tachiwana, Y. Takizawa, W. Kagawa, H. Kitao, N. Dohmae, et al. 2012. Histone chaperone activity of Fanconi anemia proteins, FANCD2 and FANCI, is required for DNA crosslink repair. *EMBO J.* 31:3524–3536. https://doi.org/10.1038/emboj.2012.197

Savage, K.I., J.J. Gorski, E.M. Barros, G.W. Irwin, L. Manti, A.J. Powell, A. Pellagatti, N. Lukashchuk, D.J. McCance, W.G. McCluggage, et al. 2014. Identification of a BRCA1-mRNA splicing complex required for efficient DNA repair and maintenance of genomic stability. *Mol. Cell.* 54:445–459. https://doi.org/10.1016/j.molcel.2014.03.021

Schlacher, K., H. Wu, and M. Jasin. 2012. A distinct replication fork protection pathway connects Fanconi anemia tumor suppressors to RAD51-BRCA1/2. *Cancer Cell.* 22:106–116. https://doi.org/10.1016/j.ccr.2012.05.015

Schwab, R.A., J. Nieminuszczy, F. Shah, J. Langton, D. Lopez Martinez, C.C. Liang, M.A. Cohn, R.J. Gibbons, A.J. Deans, and W. Niedzwiedz. 2015. The Fanconi anemia pathway maintains genome stability by coordinating replication and transcription. *Mol. Cell.* 60:351–361. https://doi.org/10.1016/j.molcel.2015.09.012

Smogorzewska, A., S. Matsuoka, P. Vinciguerra, E.R. McDonald III, K.E. Hurov, J. Luo, B.A. Ballif, S.P. Gygi, K. Hofmann, A.D. D'Andrea, and S.J. Elledge. 2007. Identification of the FANCI protein, a monoubiquitinated FANCD2 paralog required for DNA repair. *Cell.* 129:289–301. https://doi.org/10.1016/j.cell.2007.03.009

Sumpter, R. Jr., S. Sirasanagandla, A.F. Fernández, Y. Wei, X. Dong, L. Franco, Z. Zou, C. Marchal, M.Y. Lee, D.W. Clapp, et al. 2016. Fanconi anemia proteins function in mitophagy and immunity. *Cell.* 165:867–881. https://doi.org/10.1016/j.cell.2016.04.006

Suzuki, H., Y. Zuo, J. Wang, M.Q. Zhang, A. Malhotra, and A. Mayeda. 2006. Characterization of RNase R-digested cellular RNA source that consists of lariat and circular RNAs from pre-mRNA splicing. *Nucleic Acids Res.* 34:e63. https://doi.org/10.1093/nar/gkl151

Swuec, P., L. Renault, A. Borg, F. Shah, V.J. Murphy, S. van Twest, B. Snijders, A.J. Deans, and A. Costa. 2017. The FA core complex contains a homo-dimeric catalytic module for the symmetric mono-ubiquitination of FANCI-FANCD2. *Cell Reports.* 18:611–623.

Tanaka, N., A. Aronova, and B. Schwer. 2007. Ntr1 activates the Prp43 helicase to trigger release of lariat-intron from the spliceosome. *Genes Dev.* 21:2312–2325. https://doi.org/10.1101/gad.1580507

Tanikawa, M., K. Sanjiv, T. Helleday, P. Herr, and O. Mortusewicz. 2016. The spliceosome U2 snRNP factors promote genome stability through distinct mechanisms; transcription of repair factors and R-loop processing. *Oncogenesis.* 5:e280. https://doi.org/10.1038/oncsis.2016.70

van Twest, S., V.J. Murphy, C. Hodson, W. Tan, P. Swuec, J.J. O'Rourke, J. Heierhorst, W. Crismani, and A.J. Deans. 2017. Mechanism of ubiquitination and deubiquitination in the Fanconi anemia pathway. *Mol. Cell.* 65:247–259.

Visconte, V., H. Makishima, J.P. Maciejewski, and R.V. Tiu. 2012. Emerging roles of the spliceosomal machinery in myelodysplastic syndromes and other hematological disorders. *Leukemia.* 26:2447–2454. https://doi.org/10.1038/leu.2012.130

Wen, X., S. Tannukit, and M.L. Paine. 2008. TFIP11 interacts with mDEAH9, an RNA helicase involved in spliceosome disassembly. *Int. J. Mol. Sci.* 9:2105–2113. https://doi.org/10.3390/ijms9112105

Wong, J.J., W. Ritchie, O.A. Ebner, M. Selbach, J.W. Wong, Y. Huang, D. Gao, N. Pinello, M. Gonzalez, K. Baidya, et al. 2013. Orchestrated intron retention regulates normal granulocyte differentiation. *Cell.* 154:583–595. https://doi.org/10.1016/j.cell.2013.06.052

Xiao, R., P. Tang, B. Yang, J. Huang, Y. Zhou, C. Shao, H. Li, H. Sun, Y. Zhang, and X.D. Fu. 2012. Nuclear matrix factor hnRNP U/SAF-A exerts a global control of alternative splicing by regulating U2 snRNP maturation. *Mol. Cell.* 45:656–668. https://doi.org/10.1016/j.molcel.2012.01.009

Yan, Z., M. Delannoy, C. Ling, D. Daee, F. Osman, P.A. Muniandy, X. Shen, A.B. Oostra, H. Du, J. Steltenpool, et al. 2010. A histone-fold complex and FANCM form a conserved DNA-remodeling complex to maintain genome stability. *Mol. Cell.* 37:865–878. https://doi.org/10.1016/j.molcel.2010.01.039

Yoshimoto, R., N. Kataoka, K. Okawa, and M. Ohno. 2009. Isolation and characterization of post-splicing lariat-intron complexes. *Nucleic Acids Res.* 37:891–902. https://doi.org/10.1093/nar/gkn1002

Zhang, H., D.E. Kozono, K.W. O'Connor, S. Vidal-Cardenas, A. Rousseau, A. Hamilton, L. Moreau, E.F. Gaudiano, J. Greenberger, G. Bagby, et al. 2016. TGF-β inhibition rescues hematopoietic stem cell defects and bone marrow failure in Fanconi anemia. *Cell Stem Cell.* 18:668–681. https://doi.org/10.1016/j.stem.2016.03.002